Cell

Article

Small-molecule GSDMD agonism in tumors stimulates antitumor immunity without toxicity

Graphical abstract

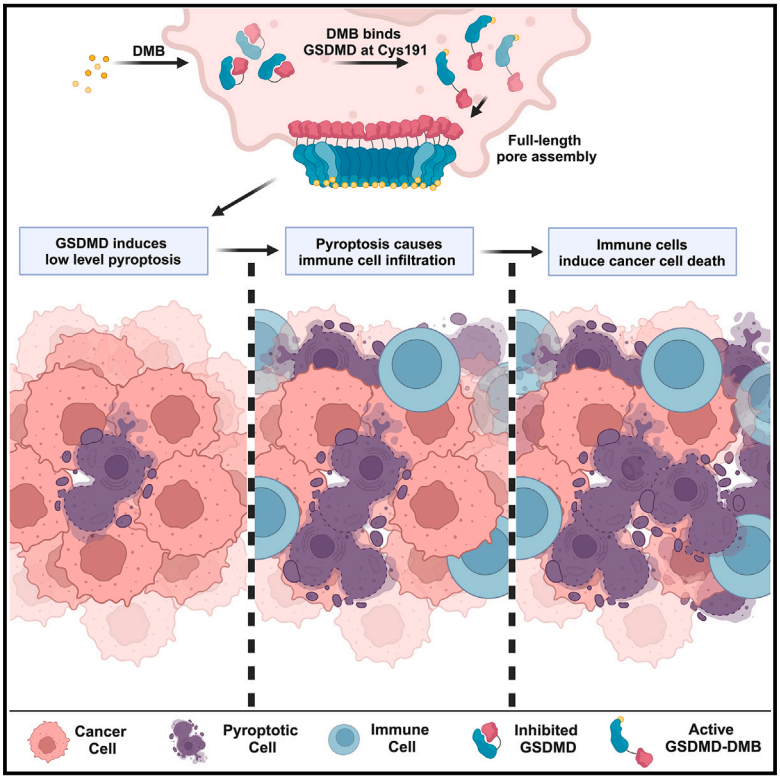

Highlights

- A GSDMD agonist (DMB) modifies Cys191 and causes cleavage-independent pyroptosis
- DMB induces antitumor immunity, dependent on GSDMD expression in tumor, not host
- Vaccination with DMB-treated tumor protects mice from tumor rechallenge
- DMB synergies with checkpoint blockade therapy, reducing cold tumor growth

Authors

Pietro Fontana, Gang Du, Ying Zhang, ..., Judith Agudo, Judy Lieberman, Hao Wu

Correspondence

judy.lieberman@childrens.harvard.edu (J.L.),
wu@crystal.harvard.edu (H.W.)

In brief

Pyroptosis is an immunogenic cell death that can promote antitumor immunity. This study identified a small molecule agonist of GSDMD that induced GSDMD pore formation and pyroptosis without cleavage and showed that pulsed and low-level pyroptosis induction in cancer cells is a strategy for cancer immunotherapy with little toxicity.

Fontana et al., 2024, Cell *187*, 1–17
October 17, 2024
https://doi.org/10.1016/j.cell.2024.08.007

CellPress

Please cite this article in press as: Fontana et al., Small-molecule GSDMD agonism in tumors stimulates antitumor immunity without toxicity, Cell (2024), https://doi.org/10.1016/j.cell.2024.08.007

Cell

CellPress

Article

Small-molecule GSDMD agonism in tumors stimulates antitumor immunity without toxicity

Pietro Fontana,[1,2,14] Gang Du,[1,2,14] Ying Zhang,[2,3,4,5,14] Haiwei Zhang,[2,3,14] Setu M. Vora,[1,2,15] Jun Jacob Hu,[1,2,12,15] Ming Shi,[1,2,6,15] Ahmet B. Tufan,[1,2] Liam B. Healy,[1,2] Shiyu Xia,[1,2,13] Dian-Jang Lee,[2,3] Zhouyihan Li,[2,3] Pilar Baldominos,[7,8] Heng Ru,[1,2,9] Hongbo R. Luo,[10,11] Judith Agudo,[7,8] Judy Lieberman,[2,3,*] and Hao Wu[1,2,16,*]

[1]Department of Biological Chemistry and Molecular Pharmacology, Harvard Medical School, Boston, MA 02115, USA
[2]Program in Cellular and Molecular Medicine, Boston Children's Hospital, Boston, MA 02115, USA
[3]Department of Pediatrics, Harvard Medical School, Boston, MA 02115, USA
[4]Key Laboratory of Cell Proliferation and Differentiation of the Ministry of Education, School of Life Sciences, Peking University, Beijing 100871, China
[5]Peking-Tsinghua Center for Life Sciences, Peking University, Beijing 100871, China
[6]School of Life Science and Technology, Harbin Institute of Technology, Harbin 150001, China
[7]Department of Cancer Immunology and Virology, Dana-Farber Cancer Institute, Boston, MA 02215, USA
[8]Department of Immunology, Harvard Medical School, Boston, MA 02215, USA
[9]Zhejiang Provincial Key Laboratory for Cancer Molecular Cell Biology, Life Sciences Institute, Zhejiang University, Hangzhou, Zhejiang 310058, China
[10]Department of Pathology, Dana-Farber/Harvard Cancer Center, Harvard Medical School, Boston, MA 02115, USA
[11]Department of Laboratory Medicine, Boston Children's Hospital, Enders Research Building, Room 814, Boston, MA 02115, USA
[12]Present address: Scorpion Therapeutics, Boston, MA 02110, USA
[13]Present address: Division of Biology and Biological Engineering, California Institute of Technology, Pasadena, CA 91125, USA
[14]These authors contributed equally
[15]These authors contributed equally
[16]Lead contact
*Correspondence: judy.lieberman@childrens.harvard.edu (J.L.), wu@crystal.harvard.edu (H.W.)
https://doi.org/10.1016/j.cell.2024.08.007

SUMMARY

Gasdermin-mediated inflammatory cell death (pyroptosis) can activate protective immunity in immunologically cold tumors. Here, we performed a high-throughput screen for compounds that could activate gasdermin D (GSDMD), which is expressed widely in tumors. We identified 6,7-dichloro-2-methylsulfonyl-3-N-tert-butylaminoquinoxaline (DMB) as a direct and selective GSDMD agonist that activates GSDMD pore formation and pyroptosis without cleaving GSDMD. In mouse tumor models, pulsed and low-level pyroptosis induced by DMB suppresses tumor growth without harming GSDMD-expressing immune cells. Protection is immune-mediated and abrogated in mice lacking lymphocytes. Vaccination with DMB-treated cancer cells protects mice from secondary tumor challenge, indicating that immunogenic cell death is induced. DMB treatment synergizes with anti-PD-1. DMB treatment does not alter circulating proinflammatory cytokine or leukocyte numbers or cause weight loss. Thus, our studies reveal a strategy that relies on a low level of tumor cell pyroptosis to induce antitumor immunity and raise the possibility of exploiting pyroptosis without causing overt toxicity.

INTRODUCTION

Immunity against neoplastic cells is critical for surveillance and control of tumor growth and metastasis. Immune protection is mediated by cytotoxic lymphocyte recognition and elimination of tumor cells as "foreign," which depends on tumor antigens, costimulation, and a danger signal. These three elements are needed to effectively activate antigen-presenting cells that phagocytose dying tumor cells, induce cytotoxic functions and cytokine secretion by cytotoxic lymphocytes, and establish long-lived memory. How a tumor cell dies shapes the immune response. Immunogenic cell death of tumor cells promotes effective immunity, while apoptosis, which can be induced by hypoxia or nutrient deprivation in the tumor environment or chemotherapy, is an immunologically silent form of cell death and sometimes even induces tolerance of tumor antigens.[1–5] The success of checkpoint blockade (CPB) and chimeric antigen receptor T cell (CAR-T) therapies has demonstrated that activating T cells to recognize cancer cells can powerfully improve cancer outcome and lead to cures.[6] Yet only a subset of cancers responds to immunotherapy. Most solid tumors are not effectively recognized by immune cells, and many tumors are devoid

Please cite this article in press as: Fontana et al., Small-molecule GSDMD agonism in tumors stimulates antitumor immunity without toxicity, Cell (2024), https://doi.org/10.1016/j.cell.2024.08.007

of functional infiltrating immune effector cells.[6,7] CPB and CAR-T therapies can also cause autoimmune side effects and cytokine release syndrome in some patients. Thus, additional therapies are needed to increase antitumor immunity specifically without activating harmful systemic side effects.

Pyroptosis is an immunogenic and inflammatory cell death mediated by the gasdermin family of pore-forming proteins.[8–13] In myeloid cells and epithelial mucosa, gasdermin D (GSDMD) can be cleaved by inflammatory caspases (1/4/5/11) downstream of pathogen or damage-induced inflammasome activation. The cleavage releases autoinhibition of the C-terminal (CT) fragment and allows the toxic N-terminal fragment (NT) of GSDMD to form pores in cell membranes, which induce inflammatory cell death to release cytosolic lactate dehydrogenase (LDH) and damage-associated molecules, such as ATP.[14] Other signaling pathways also cleave and activate gasdermins, from caspase-8 and caspase-3 to granzymes (Gzm) and neutrophil elastase.[15–27] Our recent study also revealed full-length GSDMD activation by palmitoylation.[28]

Several lines of evidence suggest that gasdermin activation in cancer cells could in principle boost antitumor immunity.[8,11] First, the importance of gasdermins in antitumor immunity is highlighted by the tumor suppressor function of GSDME, which is frequently silenced or mutated in cancers. Exogenous GSDME expression in tumors enhances the function of tumor-infiltrating killer cells, likely due to GSDME cleavage and activation by cytotoxic T lymphocyte (CTL)-delivered GzmB, which triggers tumor cell pyroptosis.[24] Second, CTL-delivered GzmA cleaves GSDMB to cause pyroptosis in GSDMB-expressing tumors and promote antitumor immunity.[21] Third, nanoparticle delivery and activation of mouse GSDMA3-NT in cancer cells heightens antitumor immunity.[12]

While these data support the beneficial role of gasdermin activation in antitumor immunity, how does one activate an endogenous gasdermin in cancer cells? To address this question, we took the hint from previous structural characterizations of full-length GSDMD in which mutations disrupting interactions of the NT and CT can lead to GSDMD constitutive activation without cleavage.[29] We hypothesized that full-length GSDMD could theoretically form membrane-permeabilizing pores and that a chemical biology approach could be used to identify activators to release the autoinhibition of an endogenous gasdermin in tumors without the need for cleavage.

Protein expression profiling of gasdermin family members showed that GSDMA, C, and E are poorly expressed in most tumors, while GSDMD and GSDMB are often expressed.[8,30] Intriguingly, GSDMB expression is associated with poor prognosis, possibly due to its additional transcriptional activity or expression of dominant negative inhibitory splice variants in tumors.[8,31–35] Here, we report the discovery of a small molecule agonist, quinoxaline 6,7-dichloro-2-methylsulfonyl-3-N-tert-butylaminoquinoxaline (DMB), that activates cleavage-independent GSDMD pore formation. Using DMB as a tool compound, we discovered that GSDMD agonism can trigger pyroptotic death of tumor cells and activate antitumor immunity in multiple mouse tumor models, without causing measurable toxicity. GSDMD expression in tumor cells, rather than host cells, is required for this activity, and agonist-treated tumor cells can act as an effective vaccine against secondary tumor challenge. When used at a lower dose (10× less), DMB synergized with anti-PD-1 to mount effective antitumor immunity in a tumor model in which DMB or anti-PD-1 alone was ineffective. These data suggest that small-molecule-mediated activation of endogenous GSDMD can act as a switch to mount effective antitumor immunity for treating GSDMD-positive cancers without inducing unnecessary inflammation or other toxicity.

RESULTS

High-throughput screen identified DMB as a potent activator of GSDMD

We performed high-throughput screening to search for GSDMD agonists using a time-resolved fluorogenic (TRF) liposome leakage assay, which detects leakage of terbium (Tb^{3+}) from Tb^{3+}-loaded liposomes incubated with GSDMD by Tb^{3+} complexation with dipicolinic acid (DPA) in the buffer (Figure 1A). In comparison with a steady-state fluorogenic assay, a TRF assay afforded by the long fluorescence lifetime of the Tb^{3+} chelate enhances sensitivity by avoiding background interference.[36] Using detergent-permeabilized liposomes as a positive control, we determined the Z′ factor, a value that measures reproducible separation of hits from controls, of this screen to be ~0.8, indicating its suitability for high-throughput screening. Over 100,000 small molecules from a Harvard ICCB-Longwood collection were screened for hit compounds that activated GSDMD pore formation to trigger liposome leakage, which was at least 50% of the total leakage caused by detergent (Figure 1B). After excluding pan-assay-interference compounds that nonspecifically react with many biological targets, GSDMD-independent liposome-disrupting compounds, auto-fluorescent compounds, and those without saturable dose-response curves, we identified 24 active compounds. One of the most potent hits was C-185, or DMB by its chemical name, which had an EC_{50} of 0.7 ± 0.0 μM (Figures 1C–1E). DMB was a potential oral drug for modulating glucagon-like peptide-1 receptor (GLP-1R) in diabetic patients but was not further developed for clinical use because it was less effective than corresponding biologics.[37–39] DMB directly bound to GSDMD by microscale thermophoresis (MST) with a dissociation constant (K_D) of 1.1 ± 0.4 μM (Figures 1F and S1A).

DMB induces pyroptosis in immortalized and primary cells in a GSDMD-dependent and cleavage-independent manner

To evaluate whether DMB activates pyroptosis in a GSDMD-dependent manner, we first used the human monocytic THP-1 cancer cell line that constitutively expresses GSDMD. Adding DMB to wild-type (WT) or GSDMD knockout (KO)[40] THP-1 cells induced significant cell death within 2 h in WT cells but minimally in GSDMD KO cells, measured by propidium iodide (PI) uptake, similar to treatment with nigericin after lipopolysaccharide (LPS) priming (Figures 2A and S1B). This distinction between WT and GSDMD KO cells was maintained throughout the time course of 24 h for both 5 or 20 μM DMB. We then measured the concentration dependence of DMB-mediated cell death and obtained an EC_{50} value of 4.8 ± 0.4 μM (Figure 2B). To determine whether

Please cite this article in press as: Fontana et al., Small-molecule GSDMD agonism in tumors stimulates antitumor immunity without toxicity, Cell (2024), https://doi.org/10.1016/j.cell.2024.08.007

CellPress

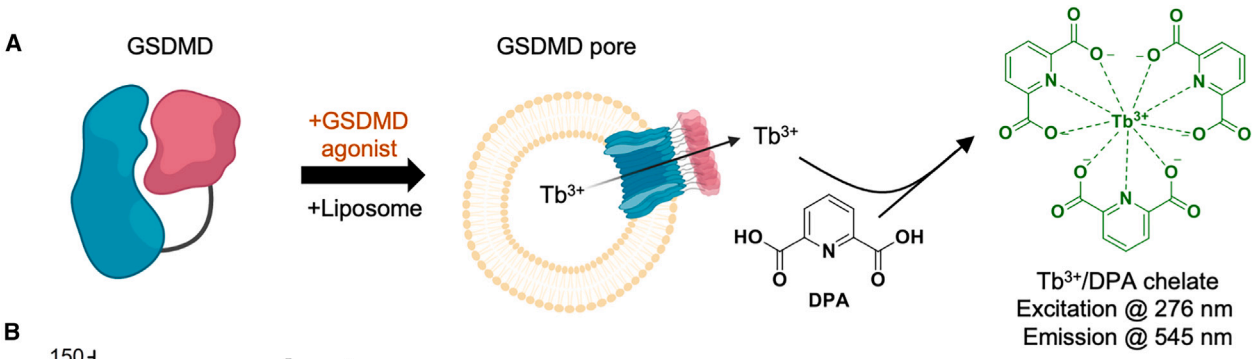

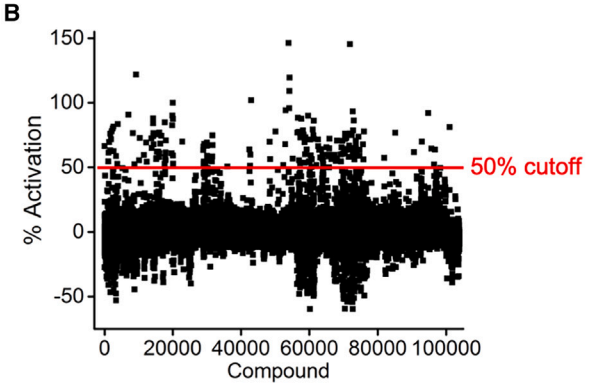

D

C-185 or

6,7-dichloro-2-methylsulfonyl-3-N-tert-butylaminoquinoxaline (DMB)

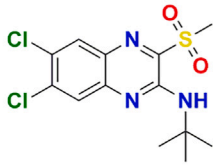

C

Hit	In vitro EC_{50} (μM)	Binding K_D by MST (μM)	Cellular activity	Hit	In vitro EC_{50} (μM)	Binding K_D by MST (μM)	Cellular activity
C-5	0.69 ± 0.10	2.90 ± 1.38	–	C-91	11.7 ± 0.98	5.38 ± 0.59	–
C-7	4.56 ± 0.53	33.4 ± 12.1	–	C-121	0.22 ± 0.01	5.33 ± 2.91	+
C-13	1.26 ± 0.03	1.86 ± 0.45	–	C-129	0.93 ± 0.07	5.60 ± 1.20	+
C-37	5.77 ± 0.18	25.8 ± 6.28	–	C-134	1.57 ± 0.17	13.1 ± 0.94	–
C-38	19.2 ± 0.50	17.5 ± 0.92	–	C-154	2.50 ± 0.06	5.35 ± 0.05	+
C-40	17.6 ± 0.26	4.82 ± 0.57	–	C-156	0.57 ± 0.04	1.89 ± 0.02	–
C-65	5.89 ± 0.14	5.96 ± 1.21	+	C-160	6.05 ± 0.68	20.2 ± 4.08	+
C-66	4.70 ± 0.21	5.48 ± 0.19	–	C-169	5.26 ± 1.54	43.8 ± 14.3	+
C-69	0.56 ± 0.02	4.92 ± 0.52	–	C-171	5.04 ± 0.61	12.7 ± 3.96	–
C-70	0.67 ± 0.03	4.89 ± 0.71	+	C-185	0.66 ± 0.01	1.05 ± 0.43	+
C-80	16.5 ± 0.86	16.8 ± 0.34	–	C-192	15.9 ± 0.44	17.1 ± 0.47	+
C-82	1.18 ± 0.06	3.31 ± 0.63	–	C-194	N.D.	N.D.	–

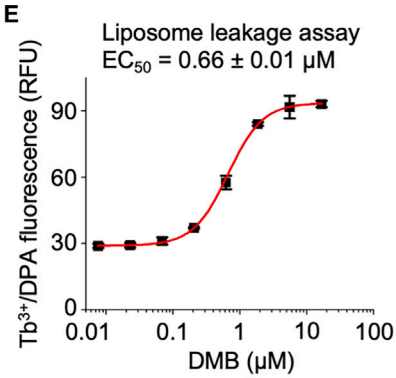

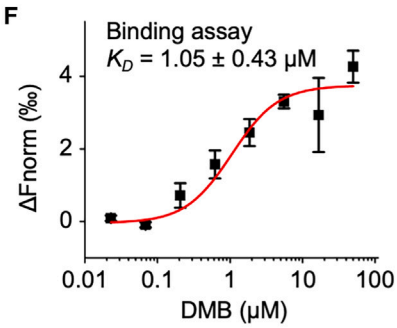

Figure 1. High-throughput screening for small-molecule GSDMD agonists

(A) GSDMD-induced liposome leakage assay using time-resolved terbium (Tb^{3+})/dipicolinic acid (DPA) fluorescence.

(B) Percentage activation of liposome leakage by screened compounds, assayed at 25 μg/mL (~50 μM for most compounds). Cutoff was 50% activation relative to detergent.

(C) The 24 identified compounds. EC_{50}s of liposome leakage, GSDMD binding dissociation constants (K_D) by microscale thermophoresis (MST), and cell death activity are shown. N.D., not detected. The data are shaded by the in vitro EC_{50}s of the compounds (red for < 1.0 μM, yellow for 1.0 - 5.0 μM, green for > 5.0 μM, and dark green for N.D.) The selected hit C-185 is labeled in red.

(D) Chemical structure of compound C-185, also known as DMB.

(E) Dose-response curve with EC_{50} of DMB in the liposome leakage assay.

(F) The binding curve for Alexa 647-labeled GSDMD with DMB by MST.

See also Figure S1.

Please cite this article in press as: Fontana et al., Small-molecule GSDMD agonism in tumors stimulates antitumor immunity without toxicity, Cell (2024), https://doi.org/10.1016/j.cell.2024.08.007

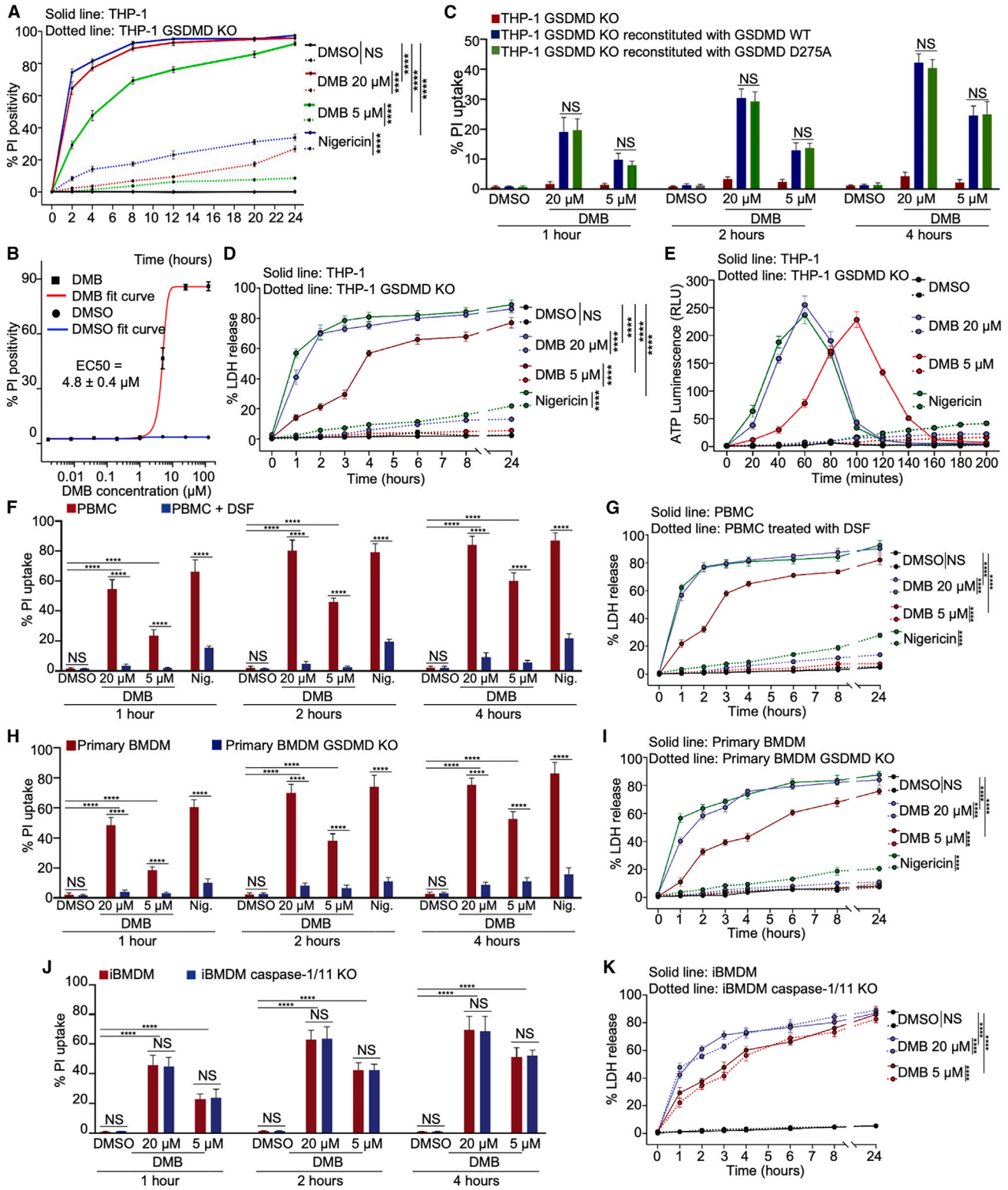

Figure 2. DMB induces pyroptotic cell death in a GSDMD-dependent manner

(A) Time course of PI positivity in WT and GSDMD KO THP-1 cells after treatment with DMSO, DMB (5 and 20 μM), or LPS + nigericin.

(B) EC_{50} determination for WT THP-1 cells using PI positivity at 4 h after treatment with different concentrations of DMB (red) or DMSO (blue).

(legend continued on next page)

Please cite this article in press as: Fontana et al., Small-molecule GSDMD agonism in tumors stimulates antitumor immunity without toxicity, Cell (2024), https://doi.org/10.1016/j.cell.2024.08.007

GSDMD cleavage was required for DMB-induced pyroptosis, we examined whether DMB can activate the D275A mutant uncleavable by inflammatory caspases or caspase-8 in GSDMD KO THP-1 cells reconstituted with WT or D275A GSDMD. After treatment with 5 or 20 μM DMB, THP-1 KO cells rescued with WT and D275A GSDMD showed comparable cell death by PI uptake at 1, 2, and 4 h (Figure 2C). These results suggested that DMB activates GSDMD independently of its cleavage.

The kinetics of killing of THP-1 cells by DMB, measured by PI uptake, LDH release, and ATP release, were similar to those of nigericin (Figures 2A, 2D, and 2E), suggesting similar mechanisms of cell death. ATP release peaked earlier than PI uptake or LDH release, suggesting that cells were dead before NINJ1 activation and plasma membrane rupture that increase dye update and LDH release.[41,42] Indeed, NINJ1 was oligomerized and released to the THP-1 supernatant upon DMB treatment, like LPS + nigericin treatment, and as expected, glycine inhibited NINJ1 oligomerization and release[42] (Figure S1C). Although membrane damage activates the NLRP3 inflammasome in monocytes or macrophages,[43] DMB treatment after LPS priming did not significantly activate NLRP3 in THP-1 cells, shown by lack of speck formation of its adaptor protein ASC or release of the cytokine interleukin-1β (IL-1β), despite inducing both PI and SYTOX Green uptake, signs of membrane permeabilization (Figure S1D). The reason for this observation is unclear, which could suggest more complexity in the relationship between membrane damage and NLRP3 activation. As expected, LPS electroporation activated the noncanonical NLRP3 inflammasome.

To evaluate the GSDMD dependence of DMB's activity in more types of cells, we treated human peripheral blood mononuclear cells (PBMCs) with DMB. DMB robustly induced PI positivity, LDH release, and ATP release in PBMCs, and pretreatment of PBMCs with the GSDMD inhibitor disulfiram (DSF)[44] strongly suppressed cell death (Figures 2F, 2G, S1E, and S1F). DMB treatment of WT and GSDMD KO primary mouse bone-marrow-derived macrophages (BMDMs) also showed that DMB induction of cell death depended on GSDMD (Figures 2H, 2I, S1G, and S1H). Similarly, DMB at both 5 and 20 μM concentrations triggered cell death in WT immortalized mouse BMDMs (iBMDMs), which was not affected by genetic ablation of both caspase-1 and caspase-11[45] (Figures 2J, 2K, S1I, and S1J), suggesting that GSDMD activation by DMB does not depend on cleavage. Because DMB reacts with a Cys residue in GSDMD (see below) and caspase-1 is a cysteine protease, we verified that DMB neither inhibited nor activated recombinant caspase-1 *in vitro* (Figure S1K).

DMB binds to GSDMD and induces cleavage-independent GSDMD oligomerization and pore formation

To examine whether DMB interacts with GSDMD in cells, we designed and synthesized two forms of biotinylated DMB, one of which (DMB-biotin) activated GSDMD in the liposome leakage assay with activity comparable to DMB (Figures 3A, S2A, and S2B). DMB-biotin pulled down endogenous GSDMD from THP-1 cell lysates, and much less GSDMD was pulled down in the presence of an excess of unlabeled DMB (Figure 3A).

We next examined the ability of DMB to induce recombinant GSDMD to form pores in liposomes. Recombinant GSDMD was incubated with DMB or an activating protease as a control in the presence of liposomes. The liposomes were then solubilized in the C12E8 detergent and examined by negative-staining electron microscopy (EM). Large pores were observed when GSDMD was cleaved by the protease or activated by DMB (Figure 3B), confirming that DMB directly induced GSDMD pore assembly. Moreover, the kinetics and extent of liposome leakage were similar whether GSDMD was activated by DMB or cleavage (Figure 3C). We next used a bioluminescence resonance energy transfer (BRET) assay that is sensitive to the distance between a yellow fluorescent protein (YFP) fused at the N terminus of GSDMD and luciferase (RLuc) fused at the C terminus to examine the effect of DMB on GSDMD autoinhibition. DMB decreased the BRET signal compared with the DMSO control (Figure 3D). Thus, these data suggest that DMB directly interacts with GSDMD *in vitro* and in cells to weaken NT-CT autoinhibition.

DMB modifies GSDMD at C191

DMB covalently modifies GLP-1R at C347 as shown by cryo-EM.[46] To understand how DMB activates GSDMD, we used nano-liquid chromatography-tandem mass spectrometry (nano-LC-MS/MS) to analyze DMB-treated recombinant human GSDMD. Tryptic fragments indicated a quinoxaline adduct of Cys191 through the carbon position 2 of DMB and the thiol of Cys191, with limited modification of other Cys residues (Figures 3E, 3F, S2C, and S2D). In fact, Cys191 is palmitoylated during inflammasome activation, which is required for GSDMD oligomerization and pore formation.[28,47–49] This Cys residue is conserved in GSDMD from different species but not in other gasdermin family members (Figure S2E). Consistently, DMB

(C) Quantification of PI uptake 1, 2, and 4 h after treatment with DMSO or DMB (5 and 20 μM) in GSDMD KO THP-1 cells, GSDMD KO THP-1 cells reconstituted with WT GSDMD, or GSDMD KO THP-1 cells reconstituted with D275A uncleavable GSDMD mutant.

(D and E) Time course of LDH release (D) and extracellular ATP measured by a luciferase-based assay (E) after treatment of WT and GSDMD KO THP-1 cells with DMSO, DMB (5 and 20 μM), or LPS + nigericin. Note discontinuous x axis in (D).

(F and G) Quantification of PI uptake (F) and LDH release (G) after treatment with DMSO, DMB (5 and 20 μM), or LPS + nigericin, with or without pretreatment with DSF in human PBMCs.

(H and I) Quantification of PI uptake (H) and LDH release (I) after treatment with DMSO, DMB (5 and 20 μM), or LPS + nigericin in WT and GSDMD KO primary mouse BMDMs.

(J and K) Quantification of PI uptake (J) and LDH release (K) after treatment of WT and caspase-1/11 KO iBMDMs with DMSO or DMB (5 and 20 μM) in mouse iBMDMs.

Error bars represent SEM of 3 independent experiments. Statistics were measured by Student's t tests (C, F, H, and J) or two-way ANOVA (A, D, G, I, and K). NS, not significant; $^{****}p < 0.0001$.

See also Figure S1.

Please cite this article in press as: Fontana et al., Small-molecule GSDMD agonism in tumors stimulates antitumor immunity without toxicity, Cell (2024), https://doi.org/10.1016/j.cell.2024.08.007

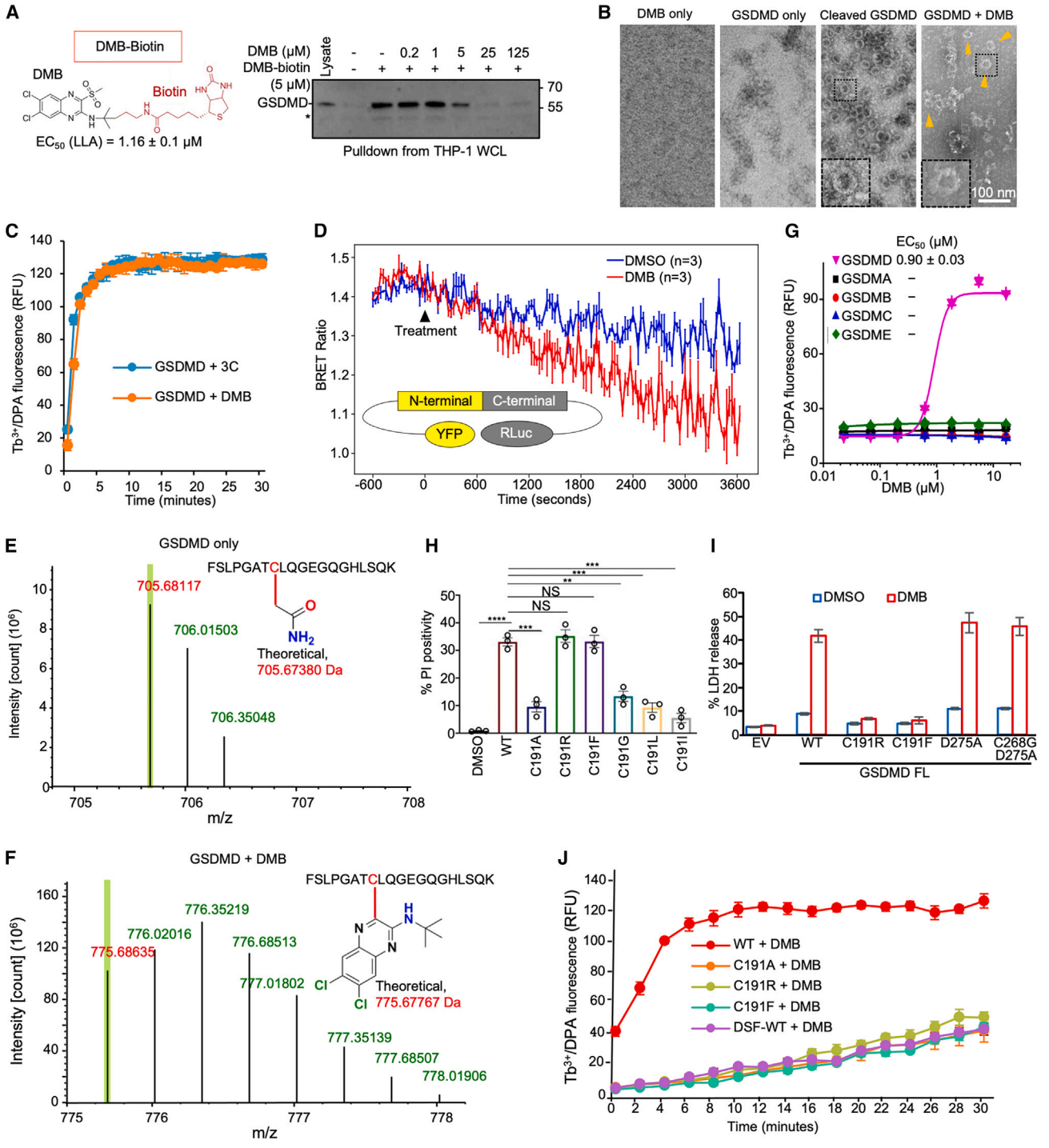

Figure 3. Cleavage-independent and selective activation of GSDMD pore formation by DMB

(A) Chemical structure of biotinylated DMB (left) and biotinylated DMB pull-down of GSDMD in THP-1 whole cell lysates (WCL), which was markedly reduced by excess DMB. The immunoblot used anti-GSDMD antibody NBP2-33422 (Novus Biologicals). * indicates a non-specific band. Lysate loaded was 5% total, and each lane is 15% total.

(B) Negative-staining EM images of liposomes incubated with DMB or GSDMD alone, cleaved GSDMD, or GSDMD plus DMB upon liposome reconstitution and detergent solubilization. Scale bars, 100 nm. Yellow arrowheads point to DMB-induced GSDMD pores. Cleaved GSDMD and DMB + GSDMD bottom left insets show enlarged images of the boxed areas.

(C) Liposome leakage assay showing that DMB activates recombinant GSDMD similarly as cleavage. The NT-CT linker contained an engineered 3C protease cleavage site.

(legend continued on next page)

Please cite this article in press as: Fontana et al., Small-molecule GSDMD agonism in tumors stimulates antitumor immunity without toxicity, Cell (2024), https://doi.org/10.1016/j.cell.2024.08.007

activated mouse GSDMD in the liposome leakage assay, albeit with ~5-fold reduced efficacy (Figure S2F), and activated human GSDMD but not other human gasdermins, suggesting that DMB acts selectively on GSDMD (Figure 3G).

To confirm that DMB targets GSDMD at Cys191, we generated GSDMD alanine mutations of Cys191 and of Cys38 as a control and evaluated them in the liposome leakage assay. Although the DMB EC_{50} values for WT and C38A GSDMD were both approximately 0.9 μM for activating GSDMD pore formation, C191A GSDMD was not activated by DMB (Figure S2G). To confirm that DMB's targeting of Cys191 of GSDMD is responsible for its effect in cells, we constructed additional Cys191 mutants of GSDMD and examined whether they caused pyroptosis, as assessed by PI uptake, when expressed in HEK293T cells. Although C191R and C191F GSDMD-NT induced cell death in HEK293T cells comparably to WT GSDMD-NT, the C191R and C191F full-length GSDMD mutants could not be activated by DMB (Figures 3H, 3I, and S2H). DMB activated WT GSDMD, the D275A mutant uncleavable by inflammatory caspases and caspase-8, or the C268G/D275A double mutant that is also uncleavable by the neutrophil elastase ELANE (Figure 3I). Consistently, DMB activation of GSDMD to permeabilize liposomes was abrogated by GSDMD pretreatment with DSF, which covalently binds to Cys191 (Figure 3J). Thus, DMB and DSF compete for the same Cys191 binding site, and DMB activates full-length GSDMD pore formation without cleavage by selectively and covalently modifying Cys191.

It was surprising that C191R and C191F GSDMD-NT induced similar levels of cell death as WT GSDMD-NT (Figure 3H). Because GSDMD-NT would have been partially palmitoylated upon transfection, we hypothesized that Arg or Phe residues partially mimics palmitoylation due to their affinity for acidic headgroups or lipid acyl chains. This mimicking effect was indeed partial, as WT GSDMD-NT induced higher levels of cell death when its palmitoylation was increased by inducing reactive oxygen species (ROS) using antimycin A (AMA) or rotenone (ROT), but C191R and C191F GSDMD-NT did not (Figures S3A and S3B). We then hypothesized that DMB also partially mimics palmitoylation due to the fairly hydrophobic nature of the compound. To test this postulate, we first examined and quantified the membrane localization of DMB-treated full-length GSDMD and compared it with GSDMD-NT under different conditions. mCherry-tagged GSDMD-NT exhibited ~60% membrane localization when transfected in HEK293T cells, which was suppressed by 2-BP treatment and increased by ROS treatment, and mCherry-tagged full-length GSDMD showed up to 88% membrane localization when treated with increasing concentrations of DMB (Figure S3C). To further dissect which step of GSDMD pore formation DMB treatment promotes, we generated structure-based oligomerization mutant (K145D/R153D) and insertion mutant (F184D/L186D) of GSDMD,[50] which were defective in cell death induction when treated with DMB (Figures S3D and S3E). We then analyzed the membrane association of recombinant WT and mutant full-length GSDMD using liposome pelleting and found that upon DMB treatment, all GSDMD samples associated with liposomes (Figure S3F), despite the reduced or abolished ability of the mutants to form pores shown by a liposome leakage assay (Figure S3G). These data suggest that like palmitoylation,[28] DMB overcomes autoinhibition and promotes membrane association.

To dissect which regions of DMB are important in agonizing GSDMD, we performed a limited structure-activity relationship (SAR) study of some DMB analogs (Figures S4A–S4C). These data showed that the methylsulfonyl moiety at position 2 was critically important, consistent with covalent bonding of DMB to GSDMD Cys191 (Figure S4D). Chemical groups at carbon positions 6 and 7 of DMB were also crucial (Figure S4E), suggesting that noncovalent interactions between DMB and GSDMD also contribute to GSDMD activation.

DMB induces pyroptosis in mouse cancer cell lines in a GSDMD-dependent manner

To study the effectiveness of DMB in mice and its GSDMD dependence, we generated GSDMD KO and GSDMD/GSDME double KO (dKO) clones of the GSDMD-expressing, cold triple-negative breast cancer line EMT6 using CRISPR-Cas9 (Figures S5A and S4B). DMB and the apoptosis-inducing chemotherapy drug mitomycin C (MMC)[51] were similarly potent at killing WT EMT6 cells *in vitro* as assessed by cell-titer Glo assay (Figure S5C). However, DMB induced the characteristic "bubble-like" cell morphology and swelling of pyroptosis and SYTOX Green uptake, while MMC induced apoptotic blebbing

(D) BRET assay using NT-fused YFP and CT-fused luciferase showing that DMB treatment reduced the intramolecular BRET ratio relative to DMSO treatment, suggesting that DMB increased the distance between the GSDMD-NT and -CT.
(E) Nano-LC/MS/MS spectrum of the Cys191-containing human GSDMD peptide (aa 184–203; 2,057.00 Da) modified on Cys191 (red) by carbamidomethyl (an increase of 57.0214 Da). A triplet-charged precursor ion m/z 705.6812 (mass: 2,114.0435 Da) was observed.
(F) The corresponding GSDMD peptide after GSDMD incubation with DMB, which was modified on Cys191 (red) by the quinoxaline moiety of DMB (an increase of 267.0330 Da). A triplet-charged precursor ion m/z 775.6767 (mass: 2,324.0591 Da) was observed.
(G) DMB dose-response curves and EC_{50} of liposome leakage after incubation with human GSDMA, GSDMB, GSDMC, GSDMD, or GSDME (0.3 μM).
(H) PI uptake in HEK293T cells transfected with WT and Cys191 mutants of GSDMD-NT. C191F and C191R GSDMD-NT induced comparable cell death as WT GSDMD-NT.
(I) LDH release from HEK293T cells transfected with full-length GSDMD and treated with DMB or DMSO. WT, the D275A mutant that cannot be cleaved by inflammatory caspases, and the C268G/D275A double mutant that also cannot be cleaved by ELANE were activated by DMB. By contrast, the C191R and C191F mutants were resistant to DMB activation.
(J) Leakage of liposomes induced by adding DMB to full-length C191A, C191R, C191F, or WT GSDMD. WT GSDMD was also pretreated with DSF before DMB treatment. Only WT GSDMD that was not pretreated with DSF could be activated by DMB.
Data represent mean ± SEM of 3 independent experiments performed in triplicate. Statistics were measured by Student's t tests (H). NS, not significant; $^{**}p < 0.01$, $^{***}p < 0.001$, $^{****}p < 0.0001$.
See also Figures S2, S3, and S4.

Please cite this article in press as: Fontana et al., Small-molecule GSDMD agonism in tumors stimulates antitumor immunity without toxicity, Cell (2024), https://doi.org/10.1016/j.cell.2024.08.007

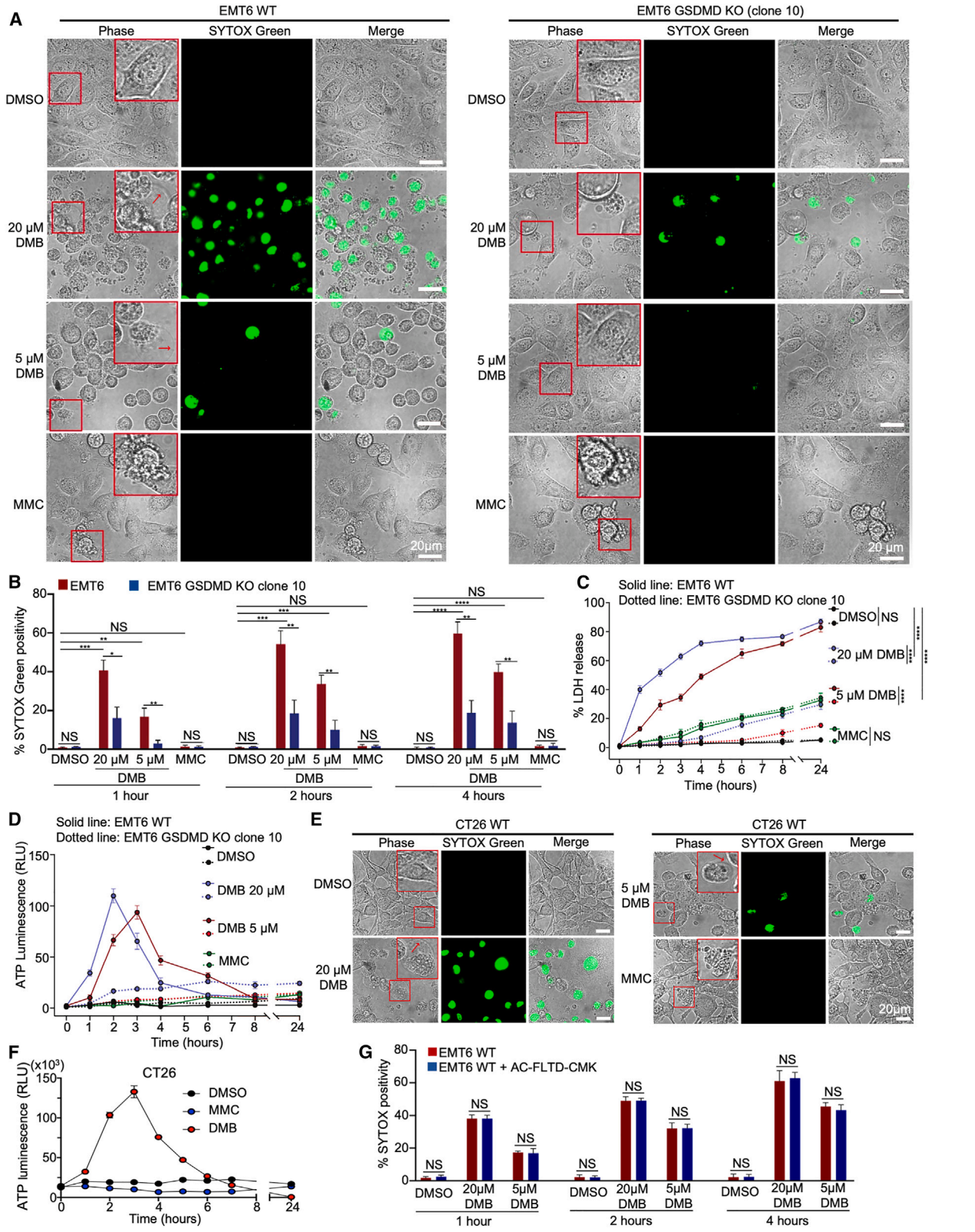

(legend on next page)

Please cite this article in press as: Fontana et al., Small-molecule GSDMD agonism in tumors stimulates antitumor immunity without toxicity, Cell (2024), https://doi.org/10.1016/j.cell.2024.08.007

with little SYTOX Green uptake (Figures 4A and 4B). DMB-treated GSDMD KO EMT6 clones exhibited much less SYTOX Green uptake than WT EMT6, shown for three independent clones (Figures 4A, 4B, S5D, and S5E). DMB also triggered release of LDH, a marker of cell membrane rupture during pyroptosis, beginning within an hour of treatment in WT but not GSDMD KO EMT6 cells (Figure 4C). GSDMD/GSDME dKO EMT6 clones were also resistant to pyroptosis by DMB measured by SYTOX Green uptake and LDH release, shown for three independent clones (Figures S5F and S5G). By contrast, MMC caused much less and delayed LDH release in WT or GSDMD KO EMT6 (Figure 4C), which might be due to secondary necrosis after apoptosis or GSDME-related conversion of apoptosis to pyroptosis since EMT6 cells express GSDME.[25] Consistently, GSDMD/GSDME dKO EMT6 cells did not release LDH upon MMC treatment (Figures S5F and S5G).

Pyroptotic cells release ATP, a damage-associated molecular pattern (DAMP).[4,52,53] We found transient ATP release into supernatants after treatment with DMB, which peaked 2 and 3 h after adding DMB to EMT6 cells, but MMC did not trigger ATP release (Figure 4D). Similarly, DMB, but not MMC, induced SYTOX Green positivity, LDH release, and ATP release in the GSDMD$^+$ colorectal carcinoma cell line CT26 (Figures 4E, 4F, S5H, and S5I). To examine if DMB-induced pyroptosis was dependent on caspases, we compared SYTOX Green uptake in the presence or absence of the inflammatory caspase inhibitor AC-FLTD-CMK (Figures 4G and S5J). Caspase inhibition did not affect DMB-induced pyroptosis in EMT6 cells. Thus, DMB rapidly induced pyroptosis and release of immunogenic DAMPs from a variety of GSDMD-expressing tumor types, independently of inflammatory caspase cleavage of GSDMD.

DMB induces tumor regression and enhances antitumor immunity that depends on GSDMD expression in the tumor

We next tested whether DMB could reduce tumor mass in syngeneic mice orthotopically implanted with EMT6 tumors. To evaluate the role of gasdermin expression in the tumor, we implanted syngeneic BALB/c mice with WT, *Gsdmd*$^{-/-}$, or *Gsdmd*$^{-/-}$*Gsdme*$^{-/-}$ EMT6 cells and treated the mice or not with 10 mg/kg DMB weekly for 2 weeks when tumors became palpable. Mice were sacrificed when any tumor exceeded the allowed size. While DMB significantly suppressed WT EMT6 tumors, *Gsdmd*$^{-/-}$ and *Gsdmd*$^{-/-}$*Gsdme*$^{-/-}$ EMT6 tumor growth was not significantly reduced by DMB (Figure 5A). A longer experiment on *Gsdmd*$^{-/-}$ EMT6 tumors also confirmed the lack of significance in the effect by DMB (Figure S6A). Although DMB did not change the numbers of tumor-infiltrating lymphocytes (TILs) in WT EMT6 tumors (Figure S6B), it significantly increased GzmB and perforin (PFN) expression and phorbol 12-myristate 13-acetate (PMA) + ionomycin-stimulated interferon (IFN)-γ and tumor necrosis factor alpha (TNF-α) production of CD8$^+$ and natural killer (NK) TILs (Figures 5B–5D). By contrast, DMB treatment of *Gsdmd*$^{-/-}$ EMT6 tumors did not significantly alter TIL number or function. A similar reduction in tumor growth and increase in CD8$^+$ and NK TIL functions without a change in TIL numbers were seen after DMB treatment of syngeneic mice bearing subcutaneous implants of CT26 colorectal cancer (Figures 5E, 5F, and S6C).

At the dose used, chosen based on preclinical studies of DMB for diabetes,[38] DMB treatment of EMT6-bearing mice did not cause systemic inflammation since plasma levels of inflammatory cytokines IL-1β, IL-18, IL-6, or TNF-α were not elevated (Figure S6D) or overt toxicity as evidenced by normal blood counts, even though monocytes and neutrophils express GSDMD (Figure S6E).

To study whether GSDMD in the host contributes to the antitumor activity of DMB, we implanted KP lung adenocarcinoma tumors subcutaneously[54] in syngeneic WT and *Gsdmd*$^{-/-}$ C57BL/6 mice since *Gsdmd*$^{-/-}$ mice were available in this background.[26] KP tumor growth was similarly inhibited, and CD8$^+$ and NK TIL functions improved in both WT and *Gsdmd*$^{-/-}$ mice (Figures 5G–5J and S6F), suggesting that GSDMD expression in host cells is dispensable for DMB's effectiveness.

DMB's direct killing is low, and its effect requires the immune system

DMB suppressed the growth of multiple tumor cell lines and activated tumor immunity *in vivo*. To examine DMB's direct cell killing and the role of immunity in tumor control, we compared the effect of DMB in immunocompetent WT and immunodeficient non-obese diabetic (NOD) scid gamma (NSG) mice that lack functional lymphocytes. Unlike in syngeneic WT mice, DMB did not suppress the growth of EMT6 tumors in NSG mice, indicating the DMB's effectiveness was immune-mediated (Figures 6A, 6B, and S6G). Next, we compared pyroptosis in EMT6 tumors of NSG and WT BALB/C mice by

Figure 4. GSDMD-dependent pyroptosis and DAMP release in mouse tumor cells

(A) Phase contrast, SYTOX Green staining, and merged images of WT (left) and GSDMD KO clone 10 (right) EMT6 cells treated for 2 h with DMSO, DMB (5 and 20 μM), or mitomycin C (MMC), an apoptosis inducer. Red squares indicate zoomed-in regions. Red arrows point to pyroptotic bubbles. Scale bars, 20 μm.

(B) Quantification of % of cells that took up SYTOX Green 1, 2, and 4 h after treatment of WT and GSDMD KO clone 10 EMT6 cells with DMSO, DMB (5 and 20 μM), or MMC.

(C and D) Time course of LDH release (C) and ATP release (D) after treatment of WT and GSDMD KO EMT6 clone 10 cells with DMSO, DMB (5 and 20 μM), or MMC.

(E) Phase contrast, SYTOX Green staining, and merged images of CT26 cells treated for 2 h with DMSO, DMB (5 and 20 μM), or mitomycin C (MMC). Red squares indicate zoomed-in regions. Red arrows point to pyroptotic bubbles. Scale bars, 20 μm.

(F) ATP release over time from CT26 cells after treatment with DMSO, MMC, or DMB. Note discontinuous x axis.

(G) % SYTOX Green uptake positivity in DMB-treated EMT6 cells that were pretreated or not with the inflammatory caspase inhibitor AC-FLTD-CMK.

Error bars represent SEM of 3 independent experiments. Statistics were measured by Student's t tests (B and G) or two-way ANOVA (C). NS, not significant; $^*p < 0.05$, $^{**}p < 0.01$, $^{***}p < 0.001$, $^{****}p < 0.0001$.

See also Figure S5.

Please cite this article in press as: Fontana et al., Small-molecule GSDMD agonism in tumors stimulates antitumor immunity without toxicity, Cell (2024), https://doi.org/10.1016/j.cell.2024.08.007

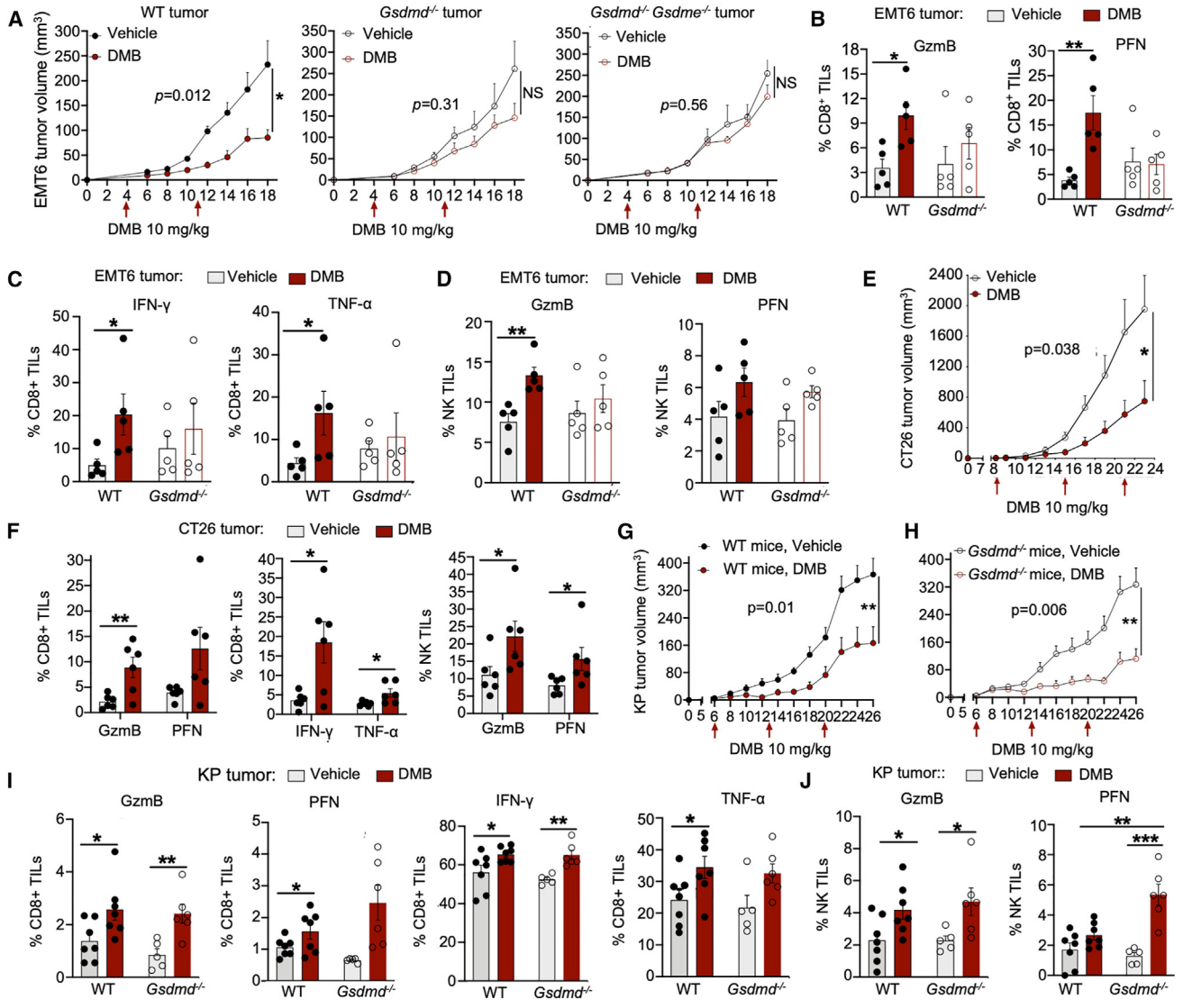

Figure 5. DMB induces antitumor activity that depends on tumor cell GSDMD expression

(A–D) Mice bearing orthotopic WT (left), *Gsdmd*$^{-/-}$ (middle), or *Gsdmd*$^{-/-}$*Gsdme*$^{-/-}$ (right) EMT6 tumors were treated with vehicle or DMB (10 mg/kg) every week starting when tumors became palpable and analyzed for tumor volume (A), percentage of CD8$^+$ TILs expressing GzmB or PFN (B), percentage of CD8$^+$ TILs expressing IFN-γ or TNF-α after PMA and ionomycin stimulation *ex vivo* (C), and percentage of NK TILs with GzmB and PFN expression (D). $n = 5$ mice/group. (E and F) Mice bearing subcutaneous CT26 tumors were treated with vehicle or DMB (10 mg/kg) and analyzed for tumor volume (E) and percentage of CD8$^+$ or NK TILs expressing GzmB or PFN and percentage of CD8$^+$ TILs expressing IFN-γ or TNF-α after PMA and ionomycin stimulation *ex vivo* (F). $n = 6$ mice/group. (G–J) Subcutaneously implanted KP tumor cells in WT or *Gsdmd*$^{-/-}$ mice treated with vehicle or DMB and analyzed for tumor volume (G and H), and percentages of CD8$^+$ (I) and NK TILs (J) expressing GzmB or PFN or expressing IFN-γ or TNF-α after PMA and ionomycin stimulation *ex vivo*. WT mice, vehicle or DMB treatment, $n = 7$ mice/group; *Gsdmd*$^{-/-}$ mice, vehicle treatment, $n = 5$ mice/group, or DMB treatment, $n = 6$ mice/group.

All data are represented as mean ± SEM. For tumor volume analysis, the area under the tumor growth curves was compared. Two-tailed Student's t tests were used to determine differences between two groups. *$p < 0.05$, **$p < 0.01$, ***$p < 0.001$.

See also Figure S6.

examining *in vivo* PI uptake in tumor cells and tumor-infiltrating immune cells in mice sacrificed 10 min after injecting PI intravenously. Strikingly, DMB caused more cell death than control in CD45$^-$ CD3$^-$ tumor cells in WT mice but not in NSG mice, while CD45$^+$ CD11b$^+$ F4/80$^+$ tumor-associated macrophages (TAMs) did not significantly increase PI uptake even in WT mice (Figures 6C and 6D). These data suggest that DMB, at the dose used, directly induced a very low level of cell death and selectively led to tumor cell death and tumor growth control due to the action of lymphocytes. We hypothesize that this is a feedforward process initiated by DMB-induced tumor cell pyroptosis and fueled by immune cell recruitment and activation that result in more pyroptosis, which in turn recruits and activates more immune cells.

Please cite this article in press as: Fontana et al., Small-molecule GSDMD agonism in tumors stimulates antitumor immunity without toxicity, Cell (2024), https://doi.org/10.1016/j.cell.2024.08.007

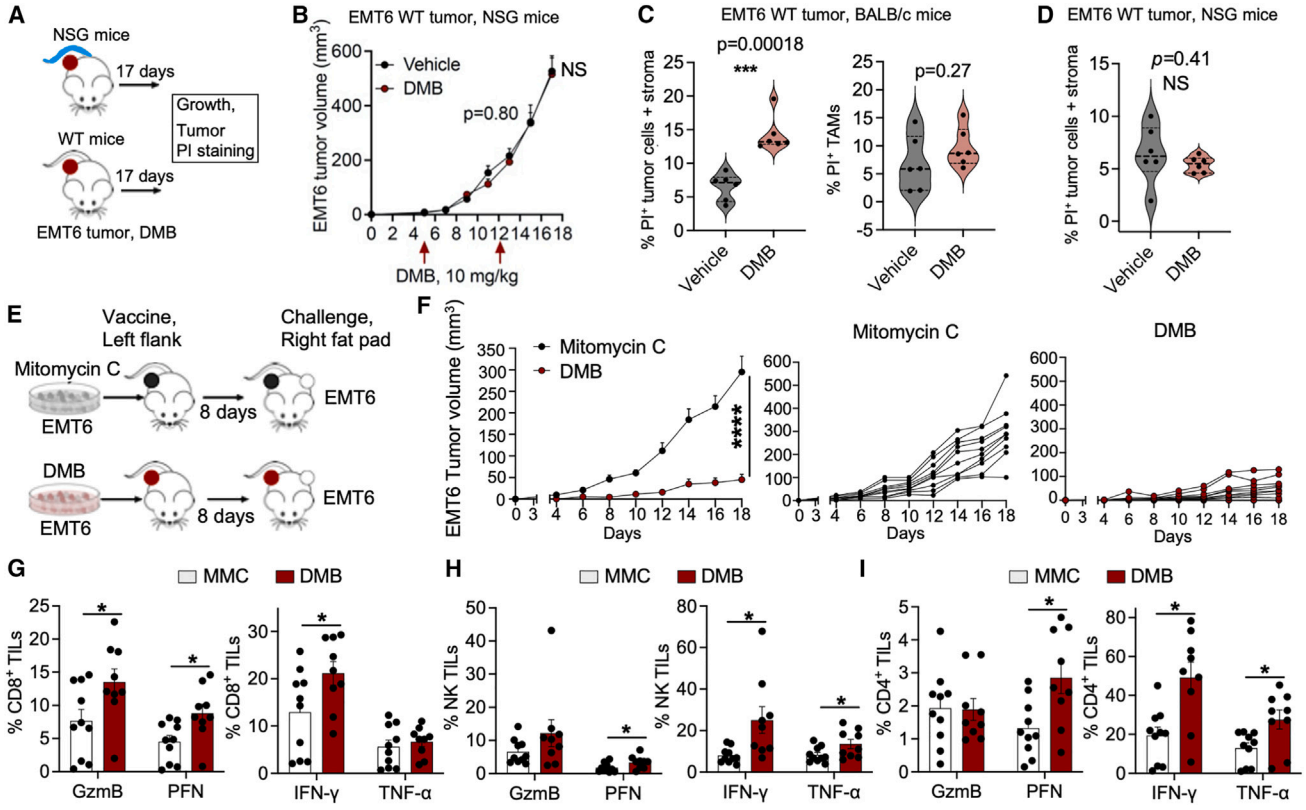

Figure 6. DMB induces immunogenic cell death, and its antitumor effect depends on the immune response

(A) Experimental scheme to analyze DMB treatment of EMT6 tumors in WT or NSG mice.

(B) DMB did not affect EMT6 tumor growth in NSG mice.

(C) EMT6 tumor cells ($CD45^-$ $CD3^-$) showed increased PI uptake in DMB-treated WT mice compared with vehicle-treated WT mice (left), but DMB did not significantly change PI uptake in $CD45^+$ $CD11b^+$ $F4/80^+$ TAMs (right).

(D) DMB treatment did not increase PI uptake of EMT6 tumor cells ($CD45^-$ $CD3^-$) in NSG mice.

(E) Schematic of vaccination experiment using MMC- or DMB-treated EMT6 tumor cells as immunogens. BALB/c mice were vaccinated in the left flank with MMC- or DMB-treated EMT6 cells and challenged 8 days later by injecting untreated EMT6 cells in the right mammary fat pad. MMC treatment, $n = 10$ mice/group; DMB treatment, $n = 12$ mice/group.

(F) Average tumor volumes (left) and individual tumor growth kinetics for MMC (middle) and DMB (right) groups.

(G–I) Percentages of $CD8^+$ (G), NK (H), and $CD4^+$ (I) TILs expressing GzmB or PFN and producing IFN-γ or TNF-α after PMA and ionomycin activation *ex vivo*. All data are represented as mean ± SEM. For tumor volume analysis, the areas under the tumor growth curves were compared. Two-tailed Student's t tests were used to determine differences between two groups. $^*p < 0.05$, $^{****}p < 0.0001$.

See also Figure S6.

DMB-treated tumor cells act as a tumor vaccine

To determine whether DMB induces immunogenic cell death, we immunized WT BALB/c mice with pyroptotic DMB-treated EMT6 cells or apoptotic MMC-treated EMT6 cells injected subcutaneously and then challenged them 8 days later with untreated EMT6 cells orthotopically injected into a mammary fat pad (Figure 6E). Immunization with DMB-treated EMT6 markedly protected mice from tumor challenge (Figure 6F). Three of 12 mice vaccinated with DMB-treated cells remained tumor-free for the duration of the study, and the remaining mice had tiny tumors, while tumors grew in all the mice immunized with MMC-treated tumors. Moreover, the tumors that grew in mice immunized with DMB-treated cells were on average 6 times smaller than those in mice immunized with MMC-treated cells. Although there was inter-animal variability in immune responses, $CD8^+$, $CD4^+$, and NK TILs in the tumors of DMB-immunized mice showed significantly increased GzmB and PFN expression and stimulated IFN-γ and TNF-α production (Figures 6G–6I). These results indicated that DMB can trigger immunogenic cell death that provides protective antitumor immunity.

DMB controls B16 tumors expressing human GSDMD

To further test the GSDMD dependence of DMB-mediated tumor control and examine whether DMB activates human GSDMD *in vivo*, we generated stable clones of B16 melanoma, which does not express endogenous *Gsdmd* (Figure S6H), by expressing a human GSDMD-GFP fusion protein or GFP alone (Figures 7A and S6I). Human GSDMD-GFP-expressing, but not the control GFP-expressing, B16 cells became sensitive to DMB-induced pyroptosis *in vitro*, as shown by PI uptake (Figures 7B and S6J). Pyroptosis occurred without GSDMD-GFP cleavage (Figure 7C).

Please cite this article in press as: Fontana et al., Small-molecule GSDMD agonism in tumors stimulates antitumor immunity without toxicity, Cell (2024), https://doi.org/10.1016/j.cell.2024.08.007

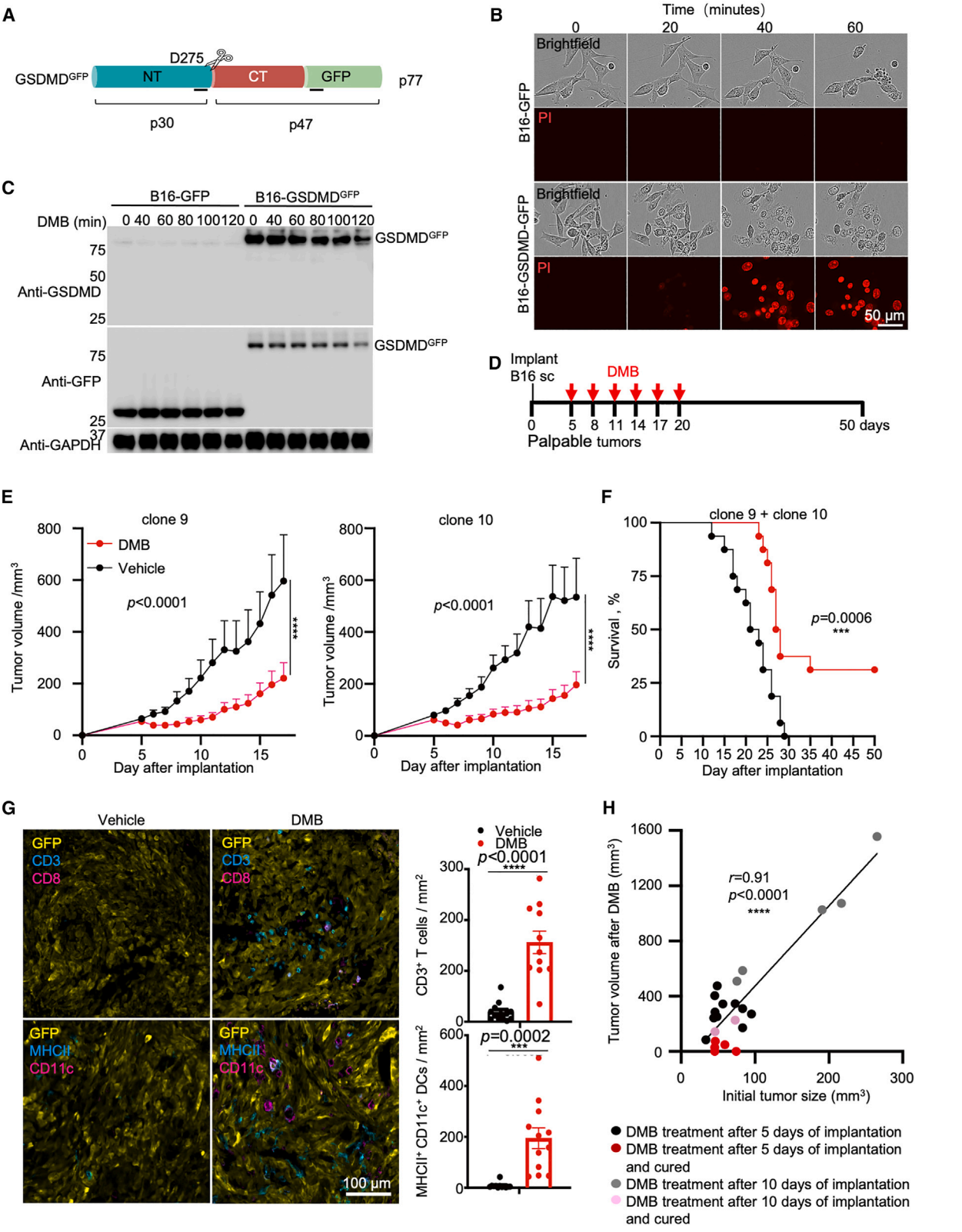

(legend on next page)

Please cite this article in press as: Fontana et al., Small-molecule GSDMD agonism in tumors stimulates antitumor immunity without toxicity, Cell (2024), https://doi.org/10.1016/j.cell.2024.08.007

Next, we inoculated the B16 clones subcutaneously into syngeneic mice and treated them with DMB every 3 days ×6 after tumors became palpable (5 days post-implantation, average tumor size 65.1 ± 21.7 mm^3) (Figure 7D). DMB strongly inhibited tumor growth and increased survival of mice implanted with B16 cells expressing human GSDMD-GFP (Figure 7E), but had no significant effect on B16 cells that expressed GFP (Figure S6K). All mice challenged with GFP-expressing B16 died (Figure S6L), as did vehicle-treated mice challenged with B16 expressing GSDMD-GFP but treated with vehicle (Figure 7F). By contrast, 5 of 16 mice bearing B16 clones expressing GSDMD-GFP that were treated with DMB survived to the end of the experiment, and 3 of these mice were cured and had no palpable tumor (Figure 7F). To examine the effect of DMB on immune cell infiltration into GSDMD-GFP-expressing tumors, we stained sections of vehicle- or DMB-treated tumors for CD3 and CD8 and for CD11c and class II major histocompatibility complex (MHCII) to label infiltrating T cells and dendritic cells (DCs), respectively (Figure 7G). The number of T cells and DCs per tumor area was highly enriched in DMB vs. vehicle-treated mice (8.3-fold more T cells, 25.2-fold more DCs). This strong effect of DMB in recruiting immune cell to B16 tumors expressing human GSDMD is in contrast to mouse tumor lines expressing endogenous mouse GSDMD (Figures S6B, S6C, and S6F), but may be consistent with the higher efficacy of DMB to human than to mouse GSDMD (Figure S2F). DMB treatment had no effect on mouse body weight (Figure S6M). These data confirm that GSDMD is required for DMB's enhanced tumor control and suggest that DMB could be effective against human tumors without causing unacceptable toxicity.

Large tumors are more difficult to control in mouse models. To investigate if DMB treatment could control larger tumors, we waited for B16-GSDMD-GFP tumors to grow for 10 days when the average tumor size was 135.8 ± 86.4 mm^3 to start DMB treatment once every 3 days for 6 times. Of the seven mice treated with DMB, two of the four mice bearing smaller tumors (45.9 and 73.0 mm^3 at time of initiating treatment) survived, whereas the remaining two mice with smaller tumors and the three mice with larger tumors (166.3 ± 83.8 mm^3 at time of initiating treatment) died (Figure 7H). A plot of the tumor sizes at the time of initiating treatment vs. tumor sizes 3 days after the 6th DMB treatment, combining mice who initiated treatment 5 and 10 days post-implantation, suggested a strong correlation between tumor size and DMB responsiveness. This finding suggests that a GSDMD agonist may need to be combined with another therapy or used only after surgery or chemotherapy to reduce tumor burden for advanced disease.

Low-dose DMB synergizes with CPB

We next asked whether DMB could induce responses to CPB in immunologically cold CPB-unresponsive 4T1E tumors. For this purpose, we used a low dose of DMB (1 mg/kg) at which DMB does not inhibit tumor growth on its own. BALB/c mice bearing palpable orthotopic tumors were treated with vehicle or anti-PD-1 every 2 days or low-dose DMB every week, alone or together. Anti-PD-1 combined with DMB, but not anti-PD-1 or DMB alone, significantly reduced tumor volume in comparison with vehicle (Figure S7A). The combined treatment significantly decreased PD-1 and CTLA-4 expression on antigen-experienced $CD44^+$ $CD8^+$ TILs, but anti-PD-1 on its own only decreased PD-1, which might have been due in part to shielding by the therapeutic antibody, which recognizes the same epitope as the staining antibody (Figure S7B). The combination of DMB and anti-PD-1 increased the percentage of $CD8^+$ and NK TILs expressing GzmB and PFN and the percentage of $CD8^+$ TILs producing IFN-γ and TNF-α after *ex vivo* stimulation (Figure S7C), without significantly changing the number of TILs or other infiltrating immune cells (Figures S7D and S7E). None of the treated mice lost weight throughout the treatment (Figure S7F),

Figure 7. DMB inhibits growth of B16 tumors expressing human GSDMD

(A) Design of the human GSDMD-GFP fusion protein ectopically expressed in B16 cells that do not express endogenous GSDMD. Black lines mark the regions of the protein recognized by the anti-GSDMD (ZRB1274, Sigma-Aldrich) and anti-GFP (2956, Cell Signaling Technology) antibodies used in (C). GFP and GSDMD-GFP were expressed in B16 cells to generate B16-GFP and B16-GSDMD-GFP cells, respectively.

(B) Time-lapse images of B16-GFP and B16-GSDMD-GFP cells treated with 10 μM DMB showing morphological changes by brightfield and PI uptake as an indicator of pyroptosis.

(C) Immunoblot of B16-GFP or B16-GSDMD-GFP incubated with 10 μM DMB for indicated times. Anti-GAPDH (60004-1-Ig, Proteintech) is a loading control. GSDMD-GFP was not cleaved by DMB.

(D) Experimental scheme for investigating the effect of DMB treatment on B16 tumors expressing human GSDMD-GFP or GFP. B16 clones were implanted subcutaneously (sc) on day 0, and mice were treated i.p. every 3 days for 6 injections (red arrows) with 10 mg/kg DMB or vehicle beginning 5 days later when all mice had palpable tumors.

(E) Growth of B16-GSDMD-GFP tumors (clone 9, left; clone 10, right) after treatment with DMB or vehicle (n = 8 mice/group). Tumor growth curves show mean ± SEM. for each timepoint and statistical analysis was performed by two-tailed Student's t test comparing the area under the tumor growth curves.

(F) Kaplan-Meier survival curve of mice bearing B16-GSDMD-GFP tumors treated with DMB or vehicle (n = 16 mice/treatment group, combining clones 9 and 10). Survival was analyzed by log-rank test. 5 of the 16 mice survived in the DMB-treated group.

(G) Immunofluorescence microscopy analysis of infiltrating $CD3^+$ $CD8^+$ T cells and $MHCII^+$ $CD11c^+$ dendritic cells in B16-GSDMD-GFP tumors after treatment with DMB or vehicle (n = 3 mice). Representative images are shown at left. Quantification is shown at right for mean ± SEM based on n = 12 images from 3 tumors for each group. Anti-CD3, anti-CD8, anti-MHCII, and CD11c antibodies were 100,235, 100,728, 107,619, and 117,309 from BioLegend.

(H) Response of B16-GSDMD-GFP tumors according to tumor size at the time of the first DMB treatment, plotted against the tumor size 3 days after the last DMB treatment. Two sets of data were included, mice treated 5 days after implantation shown in (D) and (E) and mice treated 10 days after implantation when the tumors were larger. Mice in the first and second groups that survived for the duration of the experiment are indicated by red and pink dots, respectively, and those that died or had to be sacrificed are indicated by black and gray dots, respectively. Simple linear regression was used to model the relationship between tumor volumes at initiation and after all DMB treatments. A Pearson's r value was used to assess correlation, and the statistical significance of the respective linear regression slope (Wald test) is shown.

See also Figures S6 and S7.

Please cite this article in press as: Fontana et al., Small-molecule GSDMD agonism in tumors stimulates antitumor immunity without toxicity, Cell (2024), https://doi.org/10.1016/j.cell.2024.08.007

suggesting no serious toxicity. Thus, combining DMB with CPB might be effective and well tolerated in some situations.

DISCUSSION

Inflammatory cell death is emerging to be an important immune mechanism that bridges innate and adaptive immunity to stimulate antitumor immunity and potentiate CPB or CAR-T cell therapy.[1–4,24,55,56] In addition, the clinical activity of some conventional and targeted antineoplastic agents currently used in humans is attributed to their role in re-establishing immune surveillance.[57] These agents often induce inflammatory or immunogenic cell death, which promotes the antitumor functions of TILs that are associated with more favorable therapeutic responses in patients with cancer.[1,7] Treatment with antineoplastic agents that do not predictably induce inflammatory cell death or antitumor immunity may be more prone to develop tumor resistance, relapse, and metastatic disease.

Our studies provide a paradigm of immunotherapy that inducing a low level of pyroptosis can stimulate antitumor immunity. Activation of GSDMD through a cleavage-independent agonist to induce pyroptotic inflammatory cell death also opens up possibilities for targeting other members of the GSDM family. DMB works by targeting Cys191 selectively on human and mouse GSDMD to trigger oligomerization and pore formation by overcoming autoinhibition. It induces GSDMD-dependent pyroptotic cell death in cancer lines within hours at μM potency, which results in plasma membrane rupture to release LDH and DAMPs, such as extracellular ATP. DMB reduces tumor burden in mice challenged with breast, colorectal, and lung tumors and melanoma and increases the cytotoxicity and cytokine secretion of tumor-infiltrating $CD8^+$ and NK cells. Tumor reduction depends on GSDMD expression in the tumor but not the host, supporting direct killing of cancer cells and tumor-autonomous activation of antitumor immunity. Importantly, DMB induces immunogenic cell death since vaccination with DMB-treated cells protected mice against subsequent tumor challenge. In addition, low-dose DMB synergized with anti-PD-1 to suppress growth of a CPB-resistant tumor. Importantly, DMB recognized human GSDMD and showed antitumor activity *in vivo* against a tumor line expressing human GSDMD.

Direct induction of pyroptosis by GSDMD agonists may have several advantages over secondary pyroptosis induction by chemo- and radiotherapy. First, tumor cell killing by chemotherapy and radiotherapy is mostly by apoptosis unless the tumor cell expresses GSDME. Apoptosis can be converted to pyroptosis if a tumor expresses GSDME, but GSDME expression in tumors is typically repressed by DNA hypermethylation. Thus, pyroptosis induction by these therapies can be useful but does not occur predictably.[11] Second, induction of pyroptosis in a small number of tumor cells can stimulate widespread antitumor immune control.[12] A low degree of pyroptosis induced directly by DMB is implied by our data since tumors implanted in NSG mice showed no significant increase in pyroptosis after treatment with DMB compared with vehicle. The strong vaccination effects from DMB-treated pyroptotic tumor cells suggest that the combined release of tumor antigens and DAMPs from pyroptotic tumor cells may be potent immunogens. Third, while radiotherapy and chemotherapy induce somatic mutations in tumor and healthy cells that can lead to drug resistance or secondary malignancies,[25,58,59] pyroptotic agonists might more precisely trigger immunogenic cell death.[60] Fourth, knowing the direct target of the GSDMD agonists could enable patient stratification depending on GSDMD expression. Fifth, the synergy of pyroptosis with anti-PD-1 or other CPB inhibitors could expand the range of immunotherapy responsive tumors. Finally, the effectiveness of GSDMD agonists against smaller tumors suggests its combination with therapies that reduce tumor burden, such as surgery, chemotherapy, and radiotherapy for advanced disease.

One concern about any immunotherapy is that it might theoretically cause systemic inflammation and toxicity. However, we did not find any evidence of DMB cytotoxicity to host immune cells, such as TAMs, which express GSDMD constitutively, or to other host cells, since treated mice showed no abnormalities in peripheral leukocyte counts, plasma inflammatory cytokines, or body weight. The minimal toxicity of DMB could be because administration of DMB only leads to direct killing of a small number of cells, tumor, or host, which is adequate to boost specific antitumor immunity but not high enough to lead to systemic inflammation. This hypothesis of amplification of tumor cell pyroptosis by killer cells is consistent with our *in vivo* pyroptosis data that DMB caused more pyroptosis in GSDMD-expressing tumor cells than in host cells. We also found no evidence that host GSDMD contributes to DMB-induced antitumor immunity since *Gsdmd*$^{-/-}$ mice retained sensitivity to the antitumor effect of DMB. Thus, our GSDMD-agonistic tool compound DMB and the mechanism of its action reveal a strategy of immunotherapy that is triggered by a low-level of pyroptosis induction.

Limitations of the study

While DMB covalently modifies GLP-1R *in vitro*,[37–39] because GLP-1R expression is mostly limited to the pancreas, and DMB has protective effects,[38,61] we expect that this cross-reactivity may not cause toxicity or inhibit DMB-mediated GSDMD agonism. Nonetheless, this cross-reactivity is worth studying. Lack of activation by DMB of full-length GSDMD C191R and C191F, which were equally active as NT when expressed in HEK293T cells, suggested that the pyroptotic effect of DMB is mediated by GSDMD agonism at residue Cys191. Interestingly, the Cys191/192 (human/mouse) residue targeted by DMB is also modified by GSDMD antagonists, including DSF, necrosulfonamide, or dimethyl fumarate, as well as by endogenous fumarate.[44,62,63] Since this residue is now known to be palmitoylated during inflammasome activation or high redox stress,[28] these antagonists likely function at least in part by competing with GSDMD palmitoylation. Here, DMB modifies Cys191 to overcome autoinhibition to activate GSDMD, and because of its hydrophobic nature, it may also partially mimic palmitoylation. Thus, it is no coincidence that Cys191 of GSDMD is the central residue targeted by inhibitors and activators alike. Nonetheless, as a Cys-reactive compound, DMB likely targets other unknown cellular targets, which need to be functionally characterized. DMB is a tool compound useful for probing the role of GSDMD activation *in vitro* and *in vivo*, and we are eager to use it and other hits we identified as a starting point for identifying GSDMD agonists with improved activity and selectivity for potential preclinical development.

RESOURCE AVAILABILITY

Lead contact

All information and requests for further resources and reagents should be directed to and will be fulfilled by the lead contact, Hao Wu, wu@crystal.harvard.edu.

Materials availability

All requests for resources and reagents should be directed to and will be fulfilled by the lead contact. All reagents will be made available on request after completion of a Materials Transfer Agreement.

Data and code availability

- This paper does not report original code.
- Any additional information required to reanalyze the data reported in this paper is available from the lead contact upon request.

ACKNOWLEDGMENTS

We thank Dr. Daniel Bachovchin for the *Gsdmd*$^{-/-}$ THP-1 cell line, Dr. Jonathan C. Kagan for the caspase-1/11 KO iBMDMs, the Harvard ICCB-Longwood Screening Facility for help with high throughput screening, the Harvard Medical School Nikon Imaging Center for help with fluorescence microscopy, and the Microscopy Resources on the North Quad (MicRoN) core facility at Harvard Medical School for help with fluorescence microscopy of tumor sections. This work was supported by the National Institutes of Health grants R01 CA287076, R01 CA240955, and K99 CA255841 to H.W., J.L., and Y.Z., respectively, and by a Boston Children's Hospital Office of Faculty Development/Basic & Clinical Translational Research Executive Committees Faculty Career Development Fellowship (to P.F.). H.Z., and J.J.H. were supported by post-doctoral fellowships from the Cancer Research Institute, S.M.V. was supported by a post-doctoral fellowship from the American Cancer Society, and D.-J.L. was supported by a Deutsche Forschungsgemeinschaft fellowship.

AUTHOR CONTRIBUTIONS

H.W. conceived the project. J.J.H. initiated the project and performed compound screening. P.F. performed biochemical assays and some cellular assays. G.D. performed cellular assays and some biochemical assays. S.M.V. and M.S. performed initial cellular validation. A.B.T., L.B.H., S.X., and H.R. helped with some experiments. Y.Z. and H.Z. carried out animal experiments with D.-J.L. and Z.L.'s help and J.L.'s supervision. P.B.F. performed immunofluorescence on mouse tumor sections under J.A.'s supervision. H.R.L. provided *Gsdmd*$^{-/-}$ mice. H.W., J.L., P.F., and G.D. wrote the manuscript with input from all authors.

DECLARATION OF INTERESTS

H.W. and J.L. are co-founders of Ventus Therapeutics. H.W., J.L., P.F., G.D., J.J.H., S.M.V., Y.Z., H.Z., and M.S. have filed an invention disclosure on DMB's antitumor effect. H.W., J.L., P.F., J.J.H., S.M.V., and H.Z. have filed an invention disclosure on DMB analogs from this study.

STAR★METHODS

Detailed methods are provided in the online version of this paper and include the following:

Received: March 22, 2022
Revised: November 14, 2023
Accepted: August 6, 2024
Published: September 6, 2024

REFERENCES

1. Galluzzi, L., Buqué, A., Kepp, O., Zitvogel, L., and Kroemer, G. (2017). Immunogenic cell death in cancer and infectious disease. Nat. Rev. Immunol. *17*, 97–111. https://doi.org/10.1038/nri.2016.107.
2. Kazama, H., Ricci, J.-E., Herndon, J.M., Hoppe, G., Green, D.R., and Ferguson, T.A. (2008). Induction of Immunological Tolerance by Apoptotic Cells Requires Caspase-Dependent Oxidation of High-Mobility Group Box-1 Protein. Immunity *29*, 21–32. https://doi.org/10.1016/j.immuni.2008.05.013.
3. Zhou, J., Wang, G., Chen, Y., Wang, H., Hua, Y., and Cai, Z. (2019). Immunogenic cell death in cancer therapy: Present and emerging inducers. J. Cell. Mol. Med. *23*, 4854–4865. https://doi.org/10.1111/jcmm.14356.
4. Krysko, D.V., Garg, A.D., Kaczmarek, A., Krysko, O., Agostinis, P., and Vandenabeele, P. (2012). Immunogenic cell death and DAMPs in cancer therapy. Nat. Rev. Cancer *12*, 860–875. https://doi.org/10.1038/nrc3380.
5. Waldman, A.D., Fritz, J.M., and Lenardo, M.J. (2020). A guide to cancer immunotherapy: from T cell basic science to clinical practice. Nat. Rev. Immunol. *20*, 651–668. https://doi.org/10.1038/s41577-020-0306-5.
6. Robert, C. (2020). A decade of immune-checkpoint inhibitors in cancer therapy. Nat. Commun. *11*, 3801. https://doi.org/10.1038/s41467-020-17670-y.
7. Ochoa de Olza, M., Navarro Rodrigo, B., Zimmermann, S., and Coukos, G. (2020). Turning up the heat on non-immunoreactive tumours: opportunities for clinical development. Lancet Oncol. *21*, e419–e430. https://doi.org/10.1016/S1470-2045(20)30234-5.
8. Liu, X., Xia, S., Zhang, Z., Wu, H., and Lieberman, J. (2021). Channelling inflammation: gasdermins in physiology and disease. Nat. Rev. Drug Discov. *20*, 384–405. https://doi.org/10.1038/s41573-021-00154-z.
9. Liu, X., Zhang, Z., Ruan, J., Pan, Y., Magupalli, V.G., Wu, H., and Lieberman, J. (2016). Inflammasome-activated gasdermin D causes pyroptosis by forming membrane pores. Nature *535*, 153–158. https://doi.org/10.1038/nature18629.
10. He, W.T., Wan, H., Hu, L., Chen, P., Wang, X., Huang, Z., Yang, Z.H., Zhong, C.Q., and Han, J. (2015). Gasdermin D is an executor of pyroptosis and required for interleukin-1beta secretion. Cell Res. *25*, 1285–1298. https://doi.org/10.1038/cr.2015.139.

11. Zhang, Z., Zhang, Y., and Lieberman, J. (2021). Lighting a Fire: Can We Harness Pyroptosis to Ignite Antitumor Immunity? Cancer Immunol. Res. *9*, 2–7. https://doi.org/10.1158/2326-6066.CIR-20-0525.

12. Wang, Q., Wang, Y., Ding, J., Wang, C., Zhou, X., Gao, W., Huang, H., Shao, F., and Liu, Z. (2020). A bioorthogonal system reveals antitumour immune function of pyroptosis. Nature *579*, 421–426. https://doi.org/10.1038/s41586-020-2079-1.

13. Shi, J., Gao, W., and Shao, F. (2017). Pyroptosis: Gasdermin-Mediated Programmed Necrotic Cell Death. Trends Biochem. Sci. *42*, 245–254. https://doi.org/10.1016/j.tibs.2016.10.004.

14. Broz, P., and Dixit, V.M. (2016). Inflammasomes: mechanism of assembly, regulation and signalling. Nat. Rev. Immunol. *16*, 407–420. https://doi.org/10.1038/nri.2016.58.

15. Zheng, D., Liwinski, T., and Elinav, E. (2020). Inflammasome activation and regulation: toward a better understanding of complex mechanisms. Cell Discov. *6*, 36. https://doi.org/10.1038/s41421-020-0167-x.

16. Sarhan, J., Liu, B.C., Muendlein, H.I., Li, P., Nilson, R., Tang, A.Y., Rongvaux, A., Bunnell, S.C., Shao, F., Green, D.R., and Poltorak, A. (2018). Caspase-8 induces cleavage of gasdermin D to elicit pyroptosis during Yersinia infection. Proc. Natl. Acad. Sci. USA *115*, E10888–E10897. https://doi.org/10.1073/pnas.1809548115.

17. Orning, P., Weng, D., Starheim, K., Ratner, D., Best, Z., Lee, B., Brooks, A., Xia, S., Wu, H., Kelliher, M.A., et al. (2018). Pathogen blockade of TAK1 triggers caspase-8-dependent cleavage of gasdermin D and cell death. Science *362*, 1064–1069. https://doi.org/10.1126/science.aau2818.

18. Demarco, B., Grayczyk, J.P., Bjanes, E., Le Roy, D.L., Tonnus, W., Assenmacher, C.-A., Radaelli, E., Fettrelet, T., Mack, V., Linkermann, A., et al. (2020). Caspase-8–dependent gasdermin D cleavage promotes antimicrobial defense but confers susceptibility to TNF-induced lethality. Sci. Adv. *6*, eabc3465. https://doi.org/10.1126/sciadv.abc3465.

19. Sollberger, G., Choidas, A., Burn, G.L., Habenberger, P., Di Lucrezia, R., Kordes, S., Menninger, S., Eickhoff, J., Nussbaumer, P., Klebl, B., et al. (2018). Gasdermin D plays a vital role in the generation of neutrophil extracellular traps. Sci. Immunol. *3*, eaar6689. https://doi.org/10.1126/sciimmunol.aar6689.

20. Chen, K.W., Monteleone, M., Boucher, D., Sollberger, G., Ramnath, D., Condon, N.D., von Pein, J.B., Broz, P., Sweet, M.J., and Schroder, K. (2018). Noncanonical inflammasome signaling elicits gasdermin D-dependent neutrophil extracellular traps. Sci. Immunol. *3*, eaar6676. https://doi.org/10.1126/sciimmunol.aar6676.

21. Zhou, Z., He, H., Wang, K., Shi, X., Wang, Y., Su, Y., Wang, Y., Li, D., Liu, W., Zhang, Y., et al. (2020). Granzyme A from cytotoxic lymphocytes cleaves GSDMB to trigger pyroptosis in target cells. Science *368*, eaaz7548. https://doi.org/10.1126/science.aaz7548.

22. Hansen, J.M., de Jong, M.F., Wu, Q., Zhang, L.S., Heisler, D.B., Alto, L.T., and Alto, N.M. (2021). Pathogenic ubiquitination of GSDMB inhibits NK cell bactericidal functions. Cell *184*, 3178–3191.e18. https://doi.org/10.1016/j.cell.2021.04.036.

23. Hou, J., Zhao, R., Xia, W., Chang, C.-W., You, Y., Hsu, J.-M., Nie, L., Chen, Y., Wang, Y.-C., Liu, C., et al. (2020). PD-L1-mediated gasdermin C expression switches apoptosis to pyroptosis in cancer cells and facilitates tumour necrosis. Nat. Cell Biol. *22*, 1264–1275. https://doi.org/10.1038/s41556-020-0575-z.

24. Zhang, Z., Zhang, Y., Xia, S., Kong, Q., Li, S., Liu, X., Junqueira, C., Meza-Sosa, K.F., Mok, T.M.Y., Ansara, J., et al. (2020). Gasdermin E suppresses tumour growth by activating anti-tumour immunity. Nature *579*, 415–420. https://doi.org/10.1038/s41586-020-2071-9.

25. Wang, Y., Gao, W., Shi, X., Ding, J., Liu, W., He, H., Wang, K., and Shao, F. (2017). Chemotherapy drugs induce pyroptosis through caspase-3 cleavage of a gasdermin. Nature *547*, 99–103. https://doi.org/10.1038/nature22393.

26. Kambara, H., Liu, F., Zhang, X., Liu, P., Bajrami, B., Teng, Y., Zhao, L., Zhou, S., Yu, H., Zhou, W., et al. (2018). Gasdermin D Exerts Anti-inflammatory Effects by Promoting Neutrophil Death. Cell Rep. *22*, 2924–2936. https://doi.org/10.1016/j.celrep.2018.02.067.

27. Deng, W., Bai, Y., Deng, F., Pan, Y., Mei, S., Zheng, Z., Min, R., Wu, Z., Li, W., Miao, R., et al. (2022). Streptococcal pyrogenic exotoxin B cleaves GSDMA and triggers pyroptosis. Nature *602*, 496–502. https://doi.org/10.1038/s41586-021-04384-4.

28. Du, G., Healy, L.B., David, L., Walker, C., El-Baba, T.J., Lutomski, C.A., Goh, B., Gu, B., Pi, X., Devant, P., et al. (2024). ROS-dependent S-palmitoylation activates cleaved and intact gasdermin D. Nature *630*, 437–446. https://doi.org/10.1038/s41586-024-07373-5.

29. Liu, Z., Wang, C., Yang, J., Zhou, B., Yang, R., Ramachandran, R., Abbott, D.W., and Xiao, T.S. (2019). Crystal Structures of the Full-Length Murine and Human Gasdermin D Reveal Mechanisms of Autoinhibition, Lipid Binding, and Oligomerization. Immunity *51*, 43–49.e4. https://doi.org/10.1016/j.immuni.2019.04.017.

30. Uhlen, M., Zhang, C., Lee, S., Sjöstedt, E., Fagerberg, L., Bidkhori, G., Benfeitas, R., Arif, M., Liu, Z., Edfors, F., et al. (2017). A pathology atlas of the human cancer transcriptome. Science *357*, eaan2507. https://doi.org/10.1126/science.aan2507.

31. Carl-McGrath, S., Schneider-Stock, R., Ebert, M., and Röcken, C. (2008). Differential expression and localisation of gasdermin-like (GSDML), a novel member of the cancer-associated GSDMDC protein family, in neoplastic and non-neoplastic gastric, hepatic, and colon tissues. Pathology *40*, 13–24. https://doi.org/10.1080/00313020701716250.

32. Hergueta-Redondo, M., Sarrió, D., Molina-Crespo, Á., Megias, D., Mota, A., Rojo-Sebastian, A., García-Sanz, P., Morales, S., Abril, S., Cano, A., et al. (2014). Gasdermin-B promotes invasion and metastasis in breast cancer cells. PLoS One *9*, e90099. https://doi.org/10.1371/journal.pone.0090099.

33. Kong, Q., Xia, S., Pan, X., Ye, K., Li, Z., Li, H., Tang, X., Sahni, N., Yi, S.S., Liu, X., et al. (2023). Alternative splicing of GSDMB modulates killer lymphocyte-triggered pyroptosis. Sci. Immunol. *8*, eadg3196. https://doi.org/10.1126/sciimmunol.adg3196.

34. Wang, C., Shivcharan, S., Tian, T., Wright, S., Ma, D., Chang, J., Li, K., Song, K., Xu, C., Rathinam, V.A., and Ruan, J. (2023). Structural basis for GSDMB pore formation and its targeting by IpaH7.8. Nature *616*, 590–597. https://doi.org/10.1038/s41586-023-05832-z.

35. Zhong, X., Zeng, H., Zhou, Z., Su, Y., Cheng, H., Hou, Y., She, Y., Feng, N., Wang, J., Shao, F., and Ding, J. (2023). Structural mechanisms for regulation of GSDMB pore-forming activity. Nature *616*, 598–605. https://doi.org/10.1038/s41586-023-05872-5.

36. Hemmilä, I., and Webb, S. (1997). Time-resolved fluorometry: an overview of the labels and core technologies for drug screening applications. Drug Discov. Today *2*, 373–381. https://doi.org/10.1016/S1359-6446(97)01080-5.

37. Knudsen, L.B., Kiel, D., Teng, M., Behrens, C., Bhumralkar, D., Kodra, J.T., Holst, J.J., Jeppesen, C.B., Johnson, M.D., de Jong, J.C., et al. (2007). Small-molecule agonists for the glucagon-like peptide 1 receptor. Proc. Natl. Acad. Sci. USA *104*, 937–942. https://doi.org/10.1073/pnas.0605701104.

38. Irwin, N., Flatt, P.R., Patterson, S., and Green, B.D. (2010). Insulin-releasing and metabolic effects of small molecule GLP-1 receptor agonist 6,7-dichloro-2-methylsulfonyl-3-N-tert-butylaminoquinoxaline. Eur. J. Pharmacol. *628*, 268–273. https://doi.org/10.1016/j.ejphar.2009.11.022.

39. Koole, C., Wootten, D., Simms, J., Valant, C., Sridhar, R., Woodman, O.L., Miller, L.J., Summers, R.J., Christopoulos, A., and Sexton, P.M. (2010). Allosteric ligands of the glucagon-like peptide 1 receptor (GLP-1R) differentially modulate endogenous and exogenous peptide responses in a pathway-selective manner: implications for drug screening. Mol. Pharmacol. *78*, 456–465. https://doi.org/10.1124/mol.110.065664.

40. Okondo, M.C., Johnson, D.C., Sridharan, R., Go, E.B., Chui, A.J., Wang, M.S., Poplawski, S.E., Wu, W., Liu, Y., Lai, J.H., et al. (2017). DPP8 and DPP9 inhibition induces pro-caspase-1-dependent monocyte and

macrophage pyroptosis. Nat. Chem. Biol. *13*, 46–53. https://doi.org/10.1038/nchembio.2229.

41. Kayagaki, N., Kornfeld, O.S., Lee, B.L., Stowe, I.B., O'Rourke, K., Li, Q., Sandoval, W., Yan, D., Kang, J., Xu, M., et al. (2021). NINJ1 mediates plasma membrane rupture during lytic cell death. Nature *591*, 131–136. https://doi.org/10.1038/s41586-021-03218-7.
42. Borges, J.P., Sætra, R.S.R., Volchuk, A., Bugge, M., Devant, P., Sporsheim, B., Kilburn, B.R., Evavold, C.L., Kagan, J.C., Goldenberg, N.M., et al. (2022). Glycine inhibits NINJ1 membrane clustering to suppress plasma membrane rupture in cell death. eLife *11*, e78609. https://doi.org/10.7554/eLife.78609.
43. Beckwith, K.S., Beckwith, M.S., Ullmann, S., Sætra, R.S., Kim, H., Marstad, A., Åsberg, S.E., Strand, T.A., Haug, M., Niederweis, M., et al. (2020). Plasma membrane damage causes NLRP3 activation and pyroptosis during Mycobacterium tuberculosis infection. Nat. Commun. *11*, 2270. https://doi.org/10.1038/s41467-020-16143-6.
44. Hu, J.J., Liu, X., Xia, S., Zhang, Z., Zhang, Y., Zhao, J., Ruan, J., Luo, X., Lou, X., Bai, Y., et al. (2020). FDA-approved disulfiram inhibits pyroptosis by blocking gasdermin D pore formation. Nat. Immunol. *21*, 736–745. https://doi.org/10.1038/s41590-020-0669-6.
45. Devant, P., Cao, A., and Kagan, J.C. (2021). Evolution-inspired redesign of the LPS receptor caspase-4 into an interleukin-1beta converting enzyme. Sci. Immunol. *6*, eabh3567. https://doi.org/10.1126/sciimmunol.abh3567.
46. Cong, Z., Chen, L.N., Ma, H., Zhou, Q., Zou, X., Ye, C., Dai, A., Liu, Q., Huang, W., Sun, X., et al. (2021). Molecular insights into ago-allosteric modulation of the human glucagon-like peptide-1 receptor. Nat. Commun. *12*, 3763. https://doi.org/10.1038/s41467-021-24058-z.
47. Zhuang, Z., Gu, J., Li, B.O., and Yang, L. (2024). Inhibition of gasdermin D palmitoylation by disulfiram is crucial for the treatment of myocardial infarction. Transl. Res. *264*, 66–75. https://doi.org/10.1016/j.trsl.2023.09.007.
48. Balasubramanian, A., Hsu, A.Y., Ghimire, L., Tahir, M., Devant, P., Fontana, P., Du, G., Liu, X., Fabin, D., Kambara, H., et al. (2024). The palmitoylation of gasdermin D directs its membrane translocation and pore formation during pyroptosis. Sci. Immunol. *9*, eadn1452. https://doi.org/10.1126/sciimmunol.adn1452.
49. Zhang, N., Zhang, J., Yang, Y., Shan, H., Hou, S., Fang, H., Ma, M., Chen, Z., Tan, L., and Xu, D. (2024). A palmitoylation-depalmitoylation relay spatiotemporally controls GSDMD activation in pyroptosis. Nat. Cell Biol. *26*, 757–769. https://doi.org/10.1038/s41556-024-01397-9.
50. Xia, S., Zhang, Z., Magupalli, V.G., Pablo, J.L., Dong, Y., Vora, S.M., Wang, L., Fu, T.-M., Jacobson, M.P., Greka, A., et al. (2021). Gasdermin D pore structure reveals preferential release of mature interleukin-1. Nature *593*, 607–611. https://doi.org/10.1038/s41586-021-03478-3.
51. Obeid, M., Tesniere, A., Ghiringhelli, F., Fimia, G.M., Apetoh, L., Perfettini, J.L., Castedo, M., Mignot, G., Panaretakis, T., Casares, N., et al. (2007). Calreticulin exposure dictates the immunogenicity of cancer cell death. Nat. Med. *13*, 54–61. https://doi.org/10.1038/nm1523.
52. Garg, A.D., Krysko, D.V., Verfaillie, T., Kaczmarek, A., Ferreira, G.B., Marysael, T., Rubio, N., Firczuk, M., Mathieu, C., Roebroek, A.J.M., et al. (2012). A novel pathway combining calreticulin exposure and ATP secretion in immunogenic cancer cell death. EMBO J. *31*, 1062–1079. https://doi.org/10.1038/emboj.2011.497.
53. Iyer, S.S., Pulskens, W.P., Sadler, J.J., Butter, L.M., Teske, G.J., Ulland, T.K., Eisenbarth, S.C., Florquin, S., Flavell, R.A., Leemans, J.C., and Sutterwala, F.S. (2009). Necrotic cells trigger a sterile inflammatory response through the Nlrp3 inflammasome. Proc. Natl. Acad. Sci. USA *106*, 20388–20393. https://doi.org/10.1073/pnas.0908698106.
54. Fitzgerald, B., Connolly, K.A., Cui, C., Fagerberg, E., Mariuzza, D.L., Hornick, N.I., Foster, G.G., William, I., Cheung, J.F., and Joshi, N.S. (2021). A mouse model for the study of anti-tumor T cell responses in Kras-driven lung adenocarcinoma. Cell Rep. Methods *1*, 100080. https://doi.org/10.1016/j.crmeth.2021.100080.
55. Newick, K., O'Brien, S., Moon, E., and Albelda, S.M. (2017). CAR T Cell Therapy for Solid Tumors. Annu. Rev. Med. *68*, 139–152. https://doi.org/10.1146/annurev-med-062315-120245.
56. O'Donnell, J.S., Teng, M.W.L., and Smyth, M.J. (2019). Cancer immunoediting and resistance to T cell-based immunotherapy. Nat. Rev. Clin. Oncol. *16*, 151–167. https://doi.org/10.1038/s41571-018-0142-8.
57. Galluzzi, L., Buqué, A., Kepp, O., Zitvogel, L., and Kroemer, G. (2015). Immunological Effects of Conventional Chemotherapy and Targeted Anticancer Agents. Cancer Cell *28*, 690–714. https://doi.org/10.1016/j.ccell.2015.10.012.
58. Hunter, K.W., Amin, R., Deasy, S., Ha, N.-H., and Wakefield, L. (2018). Genetic insights into the morass of metastatic heterogeneity. Nat. Rev. Cancer *18*, 211–223. https://doi.org/10.1038/nrc.2017.126.
59. Liu, J., Dang, H., and Wang, X.W. (2018). The significance of intertumor and intratumor heterogeneity in liver cancer. Exp. Mol. Med. *50*, e416. https://doi.org/10.1038/emm.2017.165.
60. Szikriszt, B., Póti, Á., Pipek, O., Krzystanek, M., Kanu, N., Molnár, J., Ribli, D., Szeltner, Z., Tusnády, G.E., Csabai, I., et al. (2016). A comprehensive survey of the mutagenic impact of common cancer cytotoxics. Genome Biol. *17*, 99. https://doi.org/10.1186/s13059-016-0963-7.
61. Zhang, H., Liu, Y., Guan, S., Qu, D., Wang, L., Wang, X., Li, X., Zhou, S., Zhou, Y., Wang, N., et al. (2016). An Orally Active Allosteric GLP-1 Receptor Agonist Is Neuroprotective in Cellular and Rodent Models of Stroke. PLoS One *11*, e0148827. https://doi.org/10.1371/journal.pone.0148827.
62. Rathkey, J.K., Zhao, J., Liu, Z., Chen, Y., Yang, J., Kondolf, H.C., Benson, B.L., Chirieleison, S.M., Huang, A.Y., Dubyak, G.R., et al. (2018). Chemical disruption of the pyroptotic pore-forming protein gasdermin D inhibits inflammatory cell death and sepsis. Sci. Immunol. *3*, eaat2738. https://doi.org/10.1126/sciimmunol.aat2738.
63. Humphries, F., Shmuel-Galia, L., Ketelut-Carneiro, N., Li, S., Wang, B., Nemmara, V.V., Wilson, R., Jiang, Z., Khalighinejad, F., Muneeruddin, K., et al. (2020). Succination inactivates gasdermin D and blocks pyroptosis. Science *369*, 1633–1637. https://doi.org/10.1126/science.abb9818.
64. Meylan, E., Dooley, A.L., Feldser, D.M., Shen, L., Turk, E., Ouyang, C., and Jacks, T. (2009). Requirement for NF-kappaB signalling in a mouse model of lung adenocarcinoma. Nature *462*, 104–107. https://doi.org/10.1038/nature08462.

Please cite this article in press as: Fontana et al., Small-molecule GSDMD agonism in tumors stimulates antitumor immunity without toxicity, Cell (2024), https://doi.org/10.1016/j.cell.2024.08.007

STAR★METHODS

KEY RESOURCES TABLE

REAGENT or RESOURCE	SOURCE	IDENTIFIER
Antibodies		
Rabbit anti-human GSDMD polyclonal antibody	Novus Biologicals	Cat# NBP2-33422; RRID: AB_2687913
Rabbit anti-mouse GSDMD polyclonal antibody	Abcam	Cat# ab209845; RRID: AB_2783550
Recombinant anti-mouse GSDMD monoclonal antibody	Sigma-Aldrich	Cat# ZRB1274
Rabbit anti-mouse GSDME monoclonal antibody	Abcam	Cat# ab215191; RRID: AB_2737000
Sheep anti-human Ninjurin-1 polyclonal antibody	R&D Systems	Cat# AF5105-SP
Anti-mouse Vinculin monoclona antibody	Millipore	Cat# SAB4200729;
Rabbit anti-GFP monoclonal antibody	Cell Signaling Technology	Cat# 2956
Mouse anti-Beta-Actin monoclonal antibody	Santa Cruz Biotechnology	Cat# sc-47778; RRID: AB_626632
Mouse anti-GAPDH monoclonal antibody	Proteintech	Cat# 60004-1-Ig
HRP-goat anti-rabbit IgG	BD Pharmingen™	Cat# 554021; RRID: AB_395213
HRP-goat anti-mouse IgG	Abcam	Cat# ab97040; RRID: AB_10698223
HRP-rabbit anti-sheep IgG	Millipore	Cat# 12-342
Anti-mouse CD11b Alexa700 monoclonal antibody	BioLegend	Cat# 101222; RRID: AB_493705
Anti-mouse CD11c APC monoclonal antibody	BioLegend	Cat# 117309; RRID: AB_313778
Anti-mouse CD16/32 TruStain FcX™ monoclonal antibody	BioLegend	Cat# 101319; RRID: AB_1574973
Anti-mouse CD3 APC monoclonal antibody	BioLegend	Cat# 100235; RRID: AB_2561455
Anti-mouse CD4 APC monoclonal antibody	BioLegend	Cat# 100515; RRID: AB_312718
Anti-mouse CD4 PE-Cy7 monoclonal antibody	BioLegend	Cat# 100527; RRID: AB_312728
Anti-mouse CD4 PerCPCy5.5 monoclonal antibody	BioLegend	Cat# 100433; RRID: AB_893330
Anti-mouse CD44 PacBlue monoclonal antibody	BioLegend	Cat# 103019; RRID: AB_493682
Anti-mouse CD44 PerCPCy5.5 monoclonal antibody	BioLegend	Cat# 103031; RRID: AB_2076206
Anti-mouse CD45 PacBlue monoclonal antibody	BioLegend	Cat# 103125; RRID: AB_493536
Anti-mouse CD45 PerCPCy5.5 monoclonal antibody	BioLegend	Cat# 103131; RRID: AB_893344
Anti-mouse CD49b FITC monoclonal antibody	BioLegend	Cat# 103503; RRID: AB_313026
Anti-mouse CD49b PacBlue monoclonal antibody	BioLegend	Cat# 108917; RRID: AB_2249376
Anti-mouse CD8a Alexa700 monoclonal antibody	BioLegend	Cat# 100729; RRID: AB_493702
Anti-mouse CD8a APC monoclonal antibody	BioLegend	Cat# 100711; RRID: AB_312750
Anti-mouse CD8a FITC monoclonal antibody	BioLegend	Cat# 100705; RRID: AB_312744
Anti-mouse CD8a PacBlue monoclonal antibody	BioLegend	Cat# 100728; RRID: AB_493426
Anti-mouse CD8a PerCPCy5.5 recombinant antibody	BioLegend	Cat# 155013; RRID: AB_2890703
Anti-mouse EpCAM PE-Cy7 monoclonal antibody	BioLegend	Cat# 118215; RRID: AB_1236477
Anti-mouse EpCAM PerCPCy5.5 monoclonal antibody	BioLegend	Cat# 118219; RRID: AB_2098647
Anti-mouse F4/80 PE-Cy7 monoclonal antibody	BioLegend	Cat# 123113; RRID: AB_893490
Anti-mouse GzmB PacBlue recombinant antibody	BioLegend	Cat# 372217; RRID: AB_2728384
Anti-mouse I-A/I-E (MHCII) PacBlue monoclonal antibody	BioLegend	Cat# 107619; RRID: AB_493528
Anti-mouse IFNγ PacBlue monoclonal antibody	BioLegend	Cat# 502521; RRID: AB_893527
Anti-mouse Ly-6G/Ly-6C(Gr-1) FITC monoclonal antibody	BioLegend	Cat# 108405; RRID: AB_313370
Anti-mouse Ly-6G/Ly-6C(Gr-1) PE monoclonal antibody	BioLegend	Cat# 108407; RRID: AB_313372
Anti-mouse NKp46 APC monoclonal antibody	BioLegend	Cat# 331917; RRID: AB_2561649
Anti-mouse PD-1 monoclonal antibody	BioXCell	Cat# BE0273; RRID: AB_2687796
Anti-mouse Perforin PE monoclonal antibody	BioLegend	Cat# 154305; RRID: AB_2721638
Anti-mouse TNF PE-Cy7 monoclonal antibody	BioLegend	Cat# 506324; RRID: AB_2204080

(*Continued on next page*)

Please cite this article in press as: Fontana et al., Small-molecule GSDMD agonism in tumors stimulates antitumor immunity without toxicity, Cell (2024), https://doi.org/10.1016/j.cell.2024.08.007

Continued

REAGENT or RESOURCE	SOURCE	IDENTIFIER
Bacterial strains		
DH5α Competent E. coli (High Efficiency)	New England Biolabs (NEB)	Cat# C2987U
BL21-CodonPlus (DE3)-RILP Competent Cells	Agilent Technologies	Cat# 230280
Chemicals, peptides, and recombinant proteins		
Ac-FLTD-CMK	MedChem Express	Cat# HY-111675
Ammonium bicarbonate	Sigma-Aldrich	Cat# A6141-1KG
Biotin	Sigma-Aldrich	Cat# B4501-1G
Biotin-DMB	This study	N/A
Blasticidin	InvivoGen	Cat# ant-bl
Cardiolipin (CL, 1',3'-bis(1,2-dioleoyl-sn-glycero-3-phospho)-sn-glycerol)	Avanti Polar Lipids	Cat# 710335C-25mg
CELLview Cell Culture Dish	USA Scientific	Cat# 5662-7870
Coelenterazine-h	Promega	Cat# S2011
Collagenase D	Sigma	Cat# 11088866001
cOmplete™ Protease Inhibitor Cocktail	Sigma	Cat# 11836170001
DAPI	Thermo Fisher	Cat# D1306
Dipicolinic acid (DPA, 2,6-Pyridinedicarboxylic acid)	Sigma	Cat# P63808-25G
Dithiothreitol (DTT)	Goldbio	Cat# DTT100
DNase I	Sigma	Cat#11284932001
Fetal bovine serum (FBS)	EMD Sciences	Cat# TMS-016-B
Formic acid (FA)	Sigma-Aldrich	Cat# F0507-100ML
Golgiplug	BD Biosciences	Cat# 555029
Iodoacetamide	Sigma-Aldrich	Cat# I6125-10G
Ionomycin	Sigma-Aldrich	Cat# I9657-1MG
IsopropylIsopropyl-β-D-thiogalactopyranoside (IPTG)	Goldbio	Cat# I2481C100
Kanamycin Monosulfate	Goldbio	Cat# K-120-100
Lipofectamine 2000	Thermo Fisher	Cat# 11668019
Lipofectamine 3000	Invitrogen	Cat# L3000008
LPS	Invivogen	Cat# tlrl-b5lps
Mitomycin C (MMC)	Cayman Chemical Company	Cat# 11435
Nigericin	Invivogen	Cat# tlrl-nig
NP-40	Sigma-Aldrich	Cat# NP40S-100ML
PE (1-palmitoyl-2-oleoyl-sn-glycero-3-phosphoethanolamine)	Avanti Polar Lipids	Cat# 850757C-25mg
Phorbol 12-myristate 13-acetate (PMA)	Sigma-Aldrich	Cat# P8139–5MG
Phosphatidic acid (PA,1,2-dioleoyl-sn-glycero-3-phosphate)	Avanti Polar Lipids	Cat# 840875C-25mg
Phosphatidylcholine (PC, 1-palmitoyl-2-oleoyl-sn-glycero-3-phosphocholine),	Avanti Polar Lipids	Cat# 850457C-25mgMG
Propidium iodide (PI)	BD Bioscience	Cat# 556463
Recombinant 3C protease	This paper	N/A
Recombinant Caspase-1	This paper	N/A
Recombinant GSDMD	This paper	N/A
Recombinant TEV protease	This paper	N/A
SYTOX Green	Thermo Fisher	Cat# S7020
Terbium(III) chloride hexahydrate (Tb^{3+})	Sigma	Cat# 204560-5G
Trypsin	Promega	Cat# VA9000
Z-YVAD-AFC	Cayman Chemical Company	Cat# 27137

(*Continued on next page*)

Please cite this article in press as: Fontana et al., Small-molecule GSDMD agonism in tumors stimulates antitumor immunity without toxicity, Cell (2024), https://doi.org/10.1016/j.cell.2024.08.007

Continued

REAGENT or RESOURCE	SOURCE	IDENTIFIER
β-mercaptoethanol	EMD Millipore	Cat# 444203-250ML
2-hydroxyl-propyl-β-cyclodextrin	Sigma-Aldrich	Cat# C0926
4–15% Mini-PROTEAN® TGX™ Precast Protein Gels, 12-well	BioRad	Cat# 4561085
4–15% Mini-PROTEAN® TGX™ Precast Protein Gels, 15-well	BioRad	Cat# 4561086
4–20% Mini-PROTEAN® TGX™ Precast Protein Gels, 10-well	BioRad	Cat# 4561094
4–20% Mini-PROTEAN® TGX™ Precast Protein Gels, 12-well	BioRad	Cat# 4561095
4–20% Mini-PROTEAN® TGX™ Precast Protein Gels, 15-well	BioRad	Cat# 4561096
6,7-dichloro-2-methylsulfonyl-3-N-tert-butylaminoquinoxaline (DMB)	Axon Medchem	Cat# Axon 1907
Critical commercial assays		
CellTiter-Glo Luminescent Cell Viability Assay	Promega	Cat# G7570
Gibson Assembly Master Mix	New England Biolabs	Cat# E2611L
KLD Enzyme Mix	New England Biolabs	Cat# M0554S
LDH-Glo Cytotoxicity Assay kit	Promega	Cat# J2380
pGuide-it-ZsGreen1 system	Takara	Cat# 632601
Pierce™ BCA Protein Assay Kit	Thermo Fisher	Cat# 23225
Q5® High-Fidelity 2X Master Mix	New England Biolabs	Cat# M0492S
QuikChange II XL site-directed mutagenesis kit	Agilent Technologies	Cat #200521
RealTime-Glo Extracellular ATP assay kit	Promega	Cat# GA5011
SuperSignal™ West Atto Ultimate Sensitivity Substrate kit	Thermo Fisher	Cat# A38556
Experimental models: Cell lines		
Human embryonic kidney 293T cells (HEK293T)	ATCC	CRL-3216
Human monocytic THP-1 cells	ATCC	TIB-202
Human monocytic THP-1 cells GSDMD KO THP-1 cells	A gift from Daniel Bachovchin, Memorial Sloan Kettering Cancer Center[40]	N/A
WT and caspase-1/11 KO iBMDMs	A gift from Jonathan C. Kagan, Boston Children's Hospital[45]	N/A
WT and GSDMD KO primary BMDMs	A gift from Jonathan C. Kagan, Boston Children's Hospital[45]	N/A
Human Peripheral Blood Mononuclear Cells (PBMC)	BPS Bioscience	79059-1
Mouse breast cancer 4T1 cells	ATCC	CRL-2539
Mouse breast cancer 4T1E cells	This study	N/A
Mouse breast cancer EMT6 cells	ATCC	CRL-2755
Mouse colon carcinoma CT26 cells	ATCC	CRL-2638
Mouse lung carcinoma KP cells	A gift from Tyler Jacks, Koch Institute for Integrative Cancer Research at MIT[64]	N/A
Mouse melanoma B16	A gift from Gordon J. Freeman, Dana-Farber Cancer Institute	N/A
Mouse melanoma B16-GFP	This study	N/A
Mouse melanoma B16-GSDMD-GFP	This study	N/A
Experimental models: Organisms/strains		
Female BALB/c mice	The Jackson Laboratory	Cat# 000651; RRID: IMSR_JAX:000651
Female C57BL/6 mice	The Jackson Laboratory	Cat# 000664; RRID: IMSR_JAX:000664
Gsdmd-/- mice	N/A	As described[26]
Oligonucleotides		
mGSDME gRNA 1 Forward: ccggAAGTGTGAGAACCATAAGAG	Integrated DNA Technology	N/A
mGSDME gRNA 1 Reverse: aaacCTCTTATGGTTCTCACACTT	Integrated DNA Technology	N/A

(*Continued on next page*)

Continued

REAGENT or RESOURCE	SOURCE	IDENTIFIER
mGSDME gRNA 2 Forward: ccggACTATACAGGTGCCACACCT	Integrated DNA Technology	N/A
mGSDME gRNA 2 Reverse: aaacAGGTGTGGCACCTGTATAGT	Integrated DNA Technology	N/A
mGSDMD gRNA 1 Forward: ccggCAGCAGAGGCGATCTCATTC	Integrated DNA Technology	N/A
mGSDMD gRNA 1 Reverse: aaacGAATGAGATCGCCTCTGCTG	Integrated DNA Technology	N/A
mGSDMD gRNA 2 Forward: ccggTCATTCCGGTGGACAGCCTG	Integrated DNA Technology	N/A
mGSDMD gRNA 2 Reverse: aaacCAGGCTGTCCACCGGAATGA	Integrated DNA Technology	N/A
Recombinant DNA		
pcDNA3.1 GSDMD-FLAG	This study	N/A
pCMV FLAG-GSDMD-NT	This study	N/A
pCMV-VSV-G	Addgene	Cat# 8454
pDB.His.MBP His-MBP-TEV-GSDMD	Xia et al.[50]	As described[50]
pDB.His.MBP His-MBP-TEV-GSDMD(NT)-3C-GSDMD(CT)	Xia et al.[50]	As described[50]
pET21a Caspase-1 P10	Xia et al.[50]	As described[50]
pET21a Caspase-1 P20	Xia et al.[50]	As described[50]
pLenti-CMV-eGFP-SV40p-BlasR	This study	N/A
pLenti-CMV-GSDMD-eGFP-SV40p-BlasR	This study	N/A
pLV Rluc-GSDMD-eYFP	This study	N/A
pSPAX2	Addgene	Cat# 12260
Software and algorithms		
Fiji ImageJ	NIH, https://doi.org/10.1038/nmeth.2019	https://fiji.sc/
GraphPad Prism 9	Graphpad	https://www.graphpad.com/scientific-software/prism/
Other		
HiTrap® SP High Performance	Cytiva	Cat# 17-1152-01
HiTrap® Q High Performance	Cytiva	Cat# 17-1154-01
Ni-NTA agarose	Qiagen	Cat# 30250
Superdex® 200 Increase 10/300 GL	Cytiva	Cat# 28-9909-44
Superose® 6 Increase 10/300 GL	Cytiva	Cat# 29-0915-96
Whatman® Nuclepore™ Track-Etched Membrane 100 nm	GE Healthcare	Cat# 800309

EXPERIMENTAL MODEL AND STUDY PARTICIPANT DETAILS

Cell lines

THP-1 and CT26 cells were grown in Roswell Park Memorial Institute (RPMI, Gibco) medium with 10% fetal bovine serum (FBS, EMD Sciences), supplemented with 100 U/ml penicillin G, 100 μg/ml streptomycin sulfate (Pen-strep, Gibco). EMT6 cells were grown in Waymouth's media (Gibco) supplemented with 15% FBS and Pen-strep. HEK293T, B16, KP, and 4T1E cells were grown in Dulbeccos Modified Eagle Medium (DMEM) with 10% FBS and Pen-Strep. B16 cell line is a gift from Gordon J. Freeman. KP cell line is a gift from Tyler Jacks. 4T1E was generated by sorting 4T1 cells (provided by Fred Miller) for high E-cadherin expression. WT and caspase-1/11 KO iBMDMs, and WT and GSDMD KO primary BMDMs are gifts from Jonathan C. Kagan. Human Peripheral Blood Mononuclear Cells (PBMCs) were purchased from BPS Bioscience. All other lines were obtained from American Type Culture Collection (ATCC) and were maintained at 37 °C under 10% CO_2.

Mice

Animal studies were conducted in compliance with the ethical regulations and were approved by the Harvard Medical School Institutional Animal Care and Use Committee. 6-8-week-old female BALB/c, C57BL/6, or NOD.Cg-*Prkdc*^{scid} *Il2rg*^{tm1Wjl}/SzJ (NSG) mice were purchased from The Jackson Laboratory and maintained at the SPF facility at Harvard Medical School. *Gsdmd*$^{-/-}$ mice in the C57BL/6 background were bred on site. All mouse experiments were conducted using protocols approved by the Animal Care and Use Committees of Boston Children's Hospital and Harvard Medical School.

Please cite this article in press as: Fontana et al., Small-molecule GSDMD agonism in tumors stimulates antitumor immunity without toxicity, Cell (2024), https://doi.org/10.1016/j.cell.2024.08.007

METHOD DETAILS

Chemical reagents

6,7-dichloro-2-methylsulfonyl-3-N-tert-butylaminoquinoxaline (DMB) was purchased from Axon MedChem. Terbium(III) chloride ($TbCl_3$), β-mercaptoethanol (2ME), dithiothreitol (DTT), dipicolinic acid (DPA), phorbol 12-myristate 13-acetate (PMA), DMSO and the cOmplete protease inhibitor cocktail were purchased from Sigma-Aldrich. Nigericin was purchased from InvivoGen.

Protein expression and purification

Full-length human GSDMD sequence was cloned into the pDB.His.MBP vector with a tobacco etch virus (TEV)-cleavable N-terminal His_6-MBP tag using NdeI and XhoI restriction sites. For expression of full-length GSDMD, *E. coli* BL21 (DE3) cells harboring the indicated plasmids were induced with 0.5 mM isopropyl-β-D-thiogalactopyranoside (IPTG) at OD_{600} of 0.8, and grown at 18 °C overnight in LB medium supplemented with 50 μg ml^{-1} kanamycin. Cells were sonicated in lysis buffer containing 40 mM HEPES at pH 7.0, 150 mM NaCl, and 5 mM imidazole. The lysate was clarified by centrifugation at 40,000 x g at 4 °C for 1 h. The supernatant containing the target protein was incubated with Ni-NTA resin (Qiagen) for 30 min at 4 °C. After incubation, the resin–supernatant mixture was poured into a column and the resin was washed with lysis buffer. The protein was eluted using the lysis buffer supplemented with 300 mM imidazole. The His_6-MBP tag was removed by overnight TEV protease digestion at 16 °C. The cleaved protein was purified using HiTrap Q ion-exchange and Superdex 200 gel-filtration columns (GE Healthcare Life Sciences).

Liposome preparation

PC (1-palmitoyl-2-oleoyl-sn-glycero-3-phosphocholine, 25 mg/mL in chloroform; 80 μL), PE (1-palmitoyl-2-oleoyl-sn-glycero-3-phosphoethanolamine, 25 mg/mL in chloroform; 128 μL) and CL [1',3'-bis(1,2-dioleoyl-*sn*-glycero-3-phospho)-*sn*-glycerol (sodium salt), 25 mg/mL in chloroform; 64 μL] were mixed and the solvent was evaporated under a stream of N_2 gas. The lipid mixture was suspended in 1 mL Buffer A (20 mM HEPES, 150 mM NaCl, 50 mM sodium citrate, and 15 mM $TbCl_3$) for 3 min. The suspension was pushed through a 100 nm Whatman® Nuclepore™ Track-Etched Membrane 30 times to obtain homogeneous liposomes. The filtered suspension was purified by size exclusion column (Superose 6, 10/300 GL) in Buffer B (20 mM HEPES, 150 mM NaCl) to remove $TbCl_3$ outside liposomes. Void fractions were pooled to produce a stock of PC/PE/CL liposomes (1.6 mM). The liposomes were diluted to 50 μM with Buffer C (20 mM HEPES, 150 mM NaCl and 50 μM DPA) for use in the high throughput screening.

TRF high-throughput screen for GSDMD agonists

Liposome leakage was detected by an increase in fluorescence when Tb^{3+} bound to DPA in Buffer C. Human GSDMD (0.3 μM) dispensed into 384-well plates (Corning 3820) was incubated with compounds from the ICCB-Longwood Screening Facility collection for 1 h before addition of PC/PE/CL liposomes (50 μM liposome lipids) to each well. The time-resolved fluorescence intensity (delay 50 μs, interval 950 μs) of each well was measured at 545 nm with an excitation of 276 nm 1 h after addition of liposomes using a Perkin Elmer EnVision plate reader. The final percent activation was calculated as $[(\text{fluorescence}_{\text{test compound}} - \text{fluorescence}_{\text{negative control}})/(\text{fluorescence}_{\text{positive control}} - \text{fluorescence}_{\text{negative control}})] \times 100$, where wells with GSDMD without agonists was used as negative control and with 0.1% SDS as positive control. 50% inhibition was arbitrarily chosen as a threshold. The hits were evaluated in concentration-response experiments in a dose range of 0.023–50 μM to determine EC_{50}.

Fluorescent protein labelling and microscale thermophoresis binding assay

Human GSDMD was labelled with AlexaFluor-647 using the Molecular Probes protein labelling kit. Ligand binding to GSDMD was evaluated using microscale thermophoresis (MST). Ligands (0.023–50 μM) were incubated with purified AlexaFluor-647-labeled protein (50 nM) for 30 min in assay buffer (20 mM HEPES at pH 7.4, 150 mM NaCl, 0.05% Tween 20). The sample was loaded into NanoTemper Monolith NT.115 glass capillaries and MST was carried out using 30% LED power and 40% MST power. K_D values were calculated using the mass action equation and NanoTemper software.

Mass spectrometry and sample preparation

Recombinant GSDMD (1 μM) was incubated with DMB (20 μM) or not for 1 h at room temperature and run on a non-reducing SDS-PAGE. The gel was stained with Coomassie blue, and the GSDMD bands were excised and placed into separate 1.5 mL polypropylene tubes. 100 μL of 50% acetonitrile in 50 mM ammonium bicarbonate buffer was added to each tube and the samples were then incubated at room temperature for 20 min. This step was repeated if necessary to destain the gel. Then, the gel slice was incubated with 55 mM iodoacetamide (in 50 mM ammonium bicarbonate) for 45 min in the dark at room temperature, before the gel was washed sequentially with 50 mM ammonium bicarbonate, water and acetonitrile. Samples were then dried in a Speedvac for 20 min. Trypsin or chymotrypsin (10 ng/μL in 25 mM ammonium bicarbonate, pH 8.0) was added to each sample tube to just cover the gel, and samples were then incubated at 37 °C for 6 h or overnight.

After digestion, samples were acidified with 0.1% formic acid (FA) and 3 μL of tryptic peptide solution was injected. Nano-LC/MS/MS was performed on a Thermo Scientific Orbitrap Fusion system, coupled with a Dionex Ultimat 3000 nano HPLC and auto sampler with 40 well standard trays. Samples were injected onto a trap column (300 μm i.d. x 5mm, C18 PepMap 100) and then onto a C18 reversed-phase nano LC column (Acclaim PepMap 100 75 μm X 25 cm), heated to 50 °C. Flow rate was set to 400 nL/min with 60 min

LC gradient, using mobile phases A (99.9% water, 0.1% FA) and B (99.9% acetonitrile, 0.1% FA). Eluted peptides were sprayed through a charged emitter tip (PicoTip Emitter, New Objective, 10 +/- 1 μm) into the mass spectrometer. Parameters were: tip voltage, +2.2 kV; Fourier Transform Mass Spectrometry (FTMS) mode for MS acquisition of precursor ions (resolution 120,000); Ion Trap Mass Spectrometry (ITMS) mode for subsequent MS/MS via higher-energy collisional dissociation (HCD) on top speed in 3 s. Proteome Discoverer 1.4 was used for protein identification and modification analysis.

Liposome pull-down assay

200 μL of recombinant GSDMD WT, oligomerization mutant (K145D, R153D), or insertion mutant (F184D, L186D) was incubated at 3 μM with 10 fold excess of DMB for 2 h at room temperature. 50 μL of liposomes (PC-PE-CL) at 1.6 mM were added to each reaction and incubated for 2 additional h at room temperature. 50 μL of each reaction was collected as a loading control. Each reaction mix was then pelleted at 4 °C for 1 h at 20,000 x g. The supernatant was removed and the pellet was resuspended in 200 μL buffer (40 mM HEPES at pH 7.0, 150 mM NaCl). Samples were resolved by SDS-PAGE and Coomassie blue staining.

Caspase-1 activity assay

To assess the effect of DMB on caspase-1 activity, we performed a fluorogenic assay using recombinant caspase-1. Caspase-1 (0.5 μM) was pre-incubated with DMB (10 μM) or not for 2 h at room temperature in a buffer containing 40 mM Hepes, pH 7.4 and 150 mM NaCl. Samples were then incubated with the fluorogenic substrate Z-YVAD-AFC (10 μM) and immediately analyzed for 2 h at 30-second intervals using a Perkin Elmer EnVision plate reader. The excitation and emission wavelengths were 400 nm and 505 nm, respectively, measured by time-resolved fluorescence (delay 50 μs, interval 950 μs) to avoid background fluorescence from DMB.

Biotin-DMB pulldown of THP-1 lysates

To investigate the binding of GSDMD to DMB in cells, we performed a biotin pull-down assay using biotin-DMB and the THP-1 cell line. For each sample, 2 million THP-1 cells were resuspended and lysed in PBS with 1% NP-40 for 20 minutes. The sample was clarified by pre-incubation with streptavidin resin for 30 minutes. The resin was removed by centrifugation at 500 x g for 2 minutes. Each sample was then incubated or not with the indicated concentration of DMB for 30 min. Subsequently, biotinylated-DMB was added to the samples and incubated for an additional 30 min. 50 μL of streptavidin resin was added to each sample and incubated for 1 h. The resin was recovered via centrifugation at 500 x g for 2 min and washed several times, including twice with 0.1% SDS in PBS, twice with PBS, once with 3 M urea in PBS, twice with PBS, and twice with water. All the steps were performed at room temperature. Finally, the samples were analyzed by western blot to determine the binding of GSDMD to DMB in THP-1 cells.

GSDMD pore reconstitution and negative-staining electron microscopy

To reconstitute GSDMD pores on liposomes, we used liposomes containing phosphatidic acid (PA), an acidic lipid, and phosphatidylcholine (PC), and an engineered human GSDMD construct previously designed for structural determination.[50] To generate liposomes, we resuspended dried lipid films consisting of 20% PA and 80% PC in Buffer D (40 mM HEPES at pH 7.0, 150 mM NaCl), extruded the liposomes through a 100-nm filter, and further purified the liposomes using a Superose 6 10/300 GL size-exclusion column equilibrated in Buffer D. The GSDMD construct contains an N-terminal TEV-removable MBP tag and a 3C protease cleavage site in place of the GSDMD inter-domain linker (L259 - D275). The MBP fusion protein was expressed in *E. coli* BL21 (DE3) and purified according to previous protocols.[50] The MBP tag was removed by TEV cleavage prior to pore reconstitution experiments. Purified GSDMD was incubated with the 3C protease or DMB in the presence of liposomes on ice overnight. Afterward, the liposomes were pelleted in an ultracentrifuge at 40,000 rpm for 1 h, and the supernatant was removed. The pellet was washed with Buffer D, and then solubilized using Buffer D supplemented with 1% C12E8 (Anatrace). Undissolved aggregates were removed by centrifugation at 15,000 rpm for 10 min at 4 °C. Clarified supernatants containing detergent-solubilized GSDMD pores (5 μL) were applied to glow-discharged Formvar-coated copper grids (Electron Microscopy Sciences), washed twice with 30 μL Buffer D supplemented with 1% C12E8, stained with 1% uranyl formate, and then blotted dry with filter paper. Imaging of the copper grids was performed using a Tecnai G2Spirit BioTWIN electron microscope (FEI) at the Electron Microscopy Facility at Harvard Medical School.

Cell viability and microscopy-based cytotoxicity assays

Lactate dehydrogenase and ATP release were measured using LDH-Glo Cytotoxicity Assay kit (Promega) and RealTime-Glo Extracellular ATP assay (Promega), respectively, according to the manufacturer's instructions. Cell viability was assessed by measuring ATP levels using the CellTiter-Glo Luminescent Cell Viability Assay (Promega, G7570) according to the manufacturer's instructions. Luminescence was measured on a BioTek Synergy 2 plate reader. For microscopy-based cytotoxicity analysis, cells were seeded in 24-well plates or CELLview Cell Culture Dishes with four compartments) (USA Scientific, 5662-7870) in culture media with 1 μg/ml propidium iodide (PI, BD Bioscience, 556463) or 0.5 μM SYTOX Green (Thermo Fisher Scientific, S7020) followed by calculating PI positivity or SYTOX Green positivity on either an Inverted Nikon Ti2 fluorescence microscope with a 40X objective (N.A. = 1.2) with a stage top incubator to maintain 37 °C and 5% CO_2 or on a Leica TCS SP8 Laser Scanning Confocal (Leica) fluorescence microscope with a heated stage to maintain 37 °C and 5% CO_2.

Please cite this article in press as: Fontana et al., Small-molecule GSDMD agonism in tumors stimulates antitumor immunity without toxicity, Cell (2024), https://doi.org/10.1016/j.cell.2024.08.007

Construct and LPS electroporation

0.24 x 10^6 THP-1 cells were electroporated with WT or D275A GSDMD constructs (1 μg) using the Neon™ Transfection System (Invitrogen) at the following setting: 1,400 volts, 20 ms pulse width and 2 pulses. 1 x 10^6 THP-1 cells were similarly electroporated with LPS (1 μg) using the same system and the same setitng. After electroporation, cells were plated in an appropriate tissue culture plate. 20 hours post-electroporation, cells were treated with indicated chemicals and assayed.

HEK293T transfection

HEK293T cells were plated in 24-well plates at 5 × 10^4 cells per well. After 20 h, WT or mutant GSDMD-NT or GSDMD-FL constructs were transfected into HEK293T cells by using Lipofectamine 3000 (Invitrogen, Cat# L3000008). 20 hours post-transfection, cells were used for assays.

Immunoblot

Cell extracts were prepared using Lysis buffer [50 mM Tris-HCl pH 7.4, 150 mM NaCl, 1% NP40 supplemented with Halt protease inhibitor cocktail (Invitrogen)]. Samples were subjected to SDS-PAGE on 4-12% Tris-Glycine gels (Bio Rad) and transferred to a nitrocellulose membrane (0.2 μm pore size) using the iBlot system (Invitrogen). The membrane was blocked in 5% milk in Tris-buffered saline containing 0.1% Tween-20 (TBST), followed by incubation with a primary antibody, extensive washing, and incubation with a secondary antibody: 1:1000 HRP-goat anti-Rabbit IgG (BD Biosciences) or 1:1000 HRP-Goat anti-mouse IgG (ab97040, abcam). Immunoblots were probed with the following primary antibodies: 1:1000 Rabbit anti-mouse GSDMD (ab209845, abcam), 1:1000 Rabbit anti-mouse GSDME (ab219151, abcam), 1:1000 Rabbit anti-human GSDMD (NBP-33422, Novus Biologicals), or 1:1000 mouse anti-Actin (C4, Santa Cruz Biotechnology), and visualized using a SuperSignal West Pico chemiluminescence ECL kit (Pierce).

Cellular imaging for membrane localization

HEK293T cells were plated in CELLview Cell Culture Dish (Four Compartments, USA Scientific, 5662-7870) at 5 x 10^4 cells per well. After 24 hours, these cells were pre-treated or not with 50 μM 2-bromopalmitate (2-BP, Sigma, 21604-1G) for 30 min, followed by transfection with GSDMD-NT-mCherry or GSDMD-FL-mCherry construct using Lipofectamine 3000 (Invitrogen, Cat # L3000008). At 20 h post-transfection, cells transfected with GSDMD-NT-mCherry were treated or not with 10 μg/mL antimycin A (AMA, Sigma, A8674), or 10 μM rotenone (Rot, Sigma, R8875-1G) for 4 hours, and fixed with 500 μL 4% paraformaldehyde (PFA) in phosphate-buffered saline (PBS) at 37 °C for 15 min. At 23 h post-transfection, cells transfected with GSDMD-FL-mCherry were treated or not with 5 or 20 μM DMB for 1 hour, and fixed with 500 μL 4% PFA in PBS at 37 °C for 15 min. After washing once with PBS (with extra care for the DMB-treated group, as cells tended to float), cells were mounted with ProLong Gold Antifade Mountant with DAPI (Thermo Fisher Scientific, P36941) and left to dry for 1.5 h in the dark. All images were taken using a Leica TCS SP8 confocal laser scanning microscope at the Boston Children's Hospital Microscopy Facility. The images were identically acquired and processed using Adobe Illustrator or Fiji/ImageJ software. Quantification of all imaging data was performed on the same microscope by counting approximately 100 cells in each of the three independent replicates.

NINJ1 oligomerization assay

2x10^6 THP-1 cells were differentiated into macrophages by 50 nM PMA treatment for 48 h. The indicated PMA-differentiated THP-1 cells were primed with LPS (1 μg/mL) for 4 h. For inflammasome activation, the indicated cells were treated with nigericin (20 μM) for 1 h. DMB-treatment was administered at 20 μM for 2 or 4 h. To prevent NINJ1 oligomerization, cells in certain conditions were pre-treated with 20 mM glycine 1 h before nigericin or DMB treatment. Cell media were collected and filtered through 0.45 μM filters and spun for 1500 rpm for 5 minutes. Supernatants were collected. Cell lysates were also obtained using RIPA buffer. Samples were subjected to SDS-PAGE electrophoresis under either reducing or non-reducing conditions. Gels were transferred to PVDF membranes using standard Towbin buffer at constant 200 mA current for 1 h and immunoblotted with the following antibodies: Ninjurin-1 (sc-136295) 1:1000 dilution, Vinculin (SAB4200729) 1:1000 dilution, Actin (sc-47778) 1:1000 dilution.

Generation of CRISPR/Cas9 knockout EMT6 lines

GSDMD and *GSMDE* CRISPR/Cas9 knockout cell lines were generated using the pGuide-it-ZsGreen1 system (Takara, Tokyo, Japan). Briefly, the selection of sgRNA target sites was performed using CHOPCHOP (https://chopchop.cbu.uib.no/). The pGuide-it-ZsGreen1/GSDMD and pGuide-it-ZsGreen1/GSDME plasmids were constructed following the manufacturer's protocol (Takara, Cat. No. 632601) using the specific oligonucleotides listed in the key resources table. The constructed plasmid was transfected into EMT6 cells using Lipofectamine® 2000 Reagent (Thermo Fisher Scientific Inc.) according to the manufacturer's instructions. After 24 h, Cas9-positive cells (marked by GFP) were sorted using a FACS Aria II flow cytometer (BD Bioscience). Clones were selected by limiting dilution and by immunoblot for lack of detectable GSDMD and/or GSDME.

Generation of B16-GFP and B16-GSDMD-GFP cell lines

Human *GSDMD* was cloned or not into the pLenti-CMV-eGFP-SV40p-BlasR plasmid for ectopic expression of GFP or GSDMD-GFP fusion protein. Lentiviruses were generated by transfecting HEK293T cells with 10 μg pLenti-CMV-eGFP-SV40p-BlasR

or pLenti-CMV-GSDMD-eGFP-SV40p-BlasR, 7.5 μg pSPAX2 and 2.5 μg pCMV-VSV-G. Supernatants collected 2 days later were used to infect B16 cells. After 2 days, 20 μg/mL blasticidin (InvivoGen) was added to select for GFP or GSDMD-GFP expressing cells. For some experiments, GSDMD-GFP-expressing clones were selected; clones were verified by flow cytometry.

Mouse experiments

CT26 cells (10^5 cells/BALB/c mouse), KP tumor cells ($2x10^5$ cells/C57BL/6 mouse) or B16-GFP pooled cells, or B16-GSDMD-GFP clones 9 or 10 ($5x10^5$ cells/C57BL/6 mouse) were injected in 50 μL of PBS subcutaneously into the right flank of mice. For orthotopic tumor challenge, EMT6 ($5x10^4$ cells/mouse) or 4T1E ($2.5x10^4$ cells/mouse) were injected into the 4th mammary fat pad of BALB/c mice. DMB working solution was prepared by diluting the stock solution 1:10 in 10% 2-hydroxyl-propyl-β-cyclodextrin/PBS (Sigma-Aldrich). Diluted DMSO was used as the vehicle control. When EMT6, CT26 or KP tumors were palpable, mice were injected intraperitoneally with the indicated concentrations of DMB once per week. For the B16 experiments, treatment was initiated either when tumors became palpable (5 days post implantation) or treatment was delayed until 10 days post-implantation. DMB was administered every 3 days x 6 treatments. In some experiments, anti-PD-1 (200 μg/mouse, clone 29F.1A12, BioXCell) was given intraperitoneally starting on day 9 after tumor challenge and every third day thereafter.

Tumor growth was monitored by measuring the perpendicular diameters of tumors every other day. For the vaccination study, EMT6 tumor cells were treated with each drug at concentrations that induced ~60-70% cell death (60 μM, 20 h for MMC and 60 μM, 5 h for DMB). Both live and dead MMC- or DMB-treated cells were collected, and each mouse was immunized by injecting 10^6 drug-treated tumor cells subcutaneously in the left flank and was challenged 8 days later by injecting $1.5x10^5$ untreated EMT6 cells in the right 4th mammary fat pad. For PI uptake assay, BALB/c or NSG mice bearing palpable EMT6 tumors were injected with PBS or 10 mg/kg DMB intraperitoneally once per week. One week following the second DMB injection, mice in the DMB treatment group were injected with another dose of DMB. 24 hours later, mice were injected intravenously with 2.5 mg/kg PI in 100 μL PBS per mouse. Mice were euthanized 10 min later, and tumors were isolated and homogenized into single cell suspensions for analysis. TAM were defined as $CD45^+$ $CD3^-$ $CD11b^+$ $F4/80^+$ cells, tumor cells (including tumor stroma) were defined as $CD45^-$ $CD3^-$ cells.

Isolation of tumor-infiltrating immune cells

Tumors were collected, cut into small pieces and treated with 2 mg/mL collagenase D, 100 μg/mL DNase I (both from Sigma) and 2% FBS in RPMI with agitation for 20 min. Tumor fragments were homogenized and filtered through 40 μm strainers, and immune cells were purified by Percoll-gradient centrifugation and washed with Leibovitz's L-15 medium.

Antibody staining and flow cytometry

Immune cells isolated from mice were stained with anti-CD45-PerCPCy5.5 or -PacBlue, CD8-PacBlue, -PerCPCy5.5, -Alexa700, -FITC or -APC, CD4-PE-Cy7, -APC or PerCPCy5.5, CD44-PerCPCy5.5 or PacBlue, Ly-6G/Ly-6C(Gr-1)-FITC or -PE, CD11b-Alexa700, CD49b-PacBlue or FITC, NKp46-APC, F4/80-PE-Cy7, EpCAM-PE-Cy7 or PerCPCy5.5. Dead cells were excluded using the live/dead fixable aqua dead cell stain. For intracellular staining of GzmB or PFN, cells were first stained with antibodies to cell-surface markers for 30 min at 4 °C, then fixed and permeabilized with fixation/permeabilization buffer and stained with anti-GzmB-PacBlue, and anti-Perforin-PE. For intracellular cytokine staining of ex vivo stimulated lymphocytes, ~10^6 cells per sample were cultured in RPMI medium containing 2% FBS and stimulated with PMA (50 ng/ml), ionomycin (2 μg/mL) and Golgiplug (1.5 μg/mL) for 4 h. Cells cultured with medium and Golgiplug alone served as negative control. Cells were then stained with antibodies to IFNγ-PacBlue or -APC and TNF-PE-Cy7 after fixation/permeabilization. Cells were analyzed by BD FACSCanto II and data were analyzed with FlowJo V.10.

Immunofluorescence imaging and quantification of B16 tumors

Tumors were harvested and fixed in fixation buffer (20% sucrose, 4% paraformaldehyde) at 4 °C overnight. The next day they were embedded in OCT compound (Sakura), solidified on dry ice. and sectioned into 10 μm sections using a microtome (Leica). Sections were blocked in 1:100 TruStain FcX (BioLegend) blocking buffer (TBS containing 10% FBS, 2% normal mouse serum, 0.1% Tween-20) for 1 h at room temperature and incubated overnight at 4 °C with fluorescently labeled anti-CD3, anti-CD8, anti-MHCII or anti-CD11c antibodies. Antibodies were used at 1:100 dilution in blocking buffer. Nuclear staining was performed with DAPI (ThermoFisher) at 1:1000 dilution in TBST for 15 min. Images were acquired using a Micron Olympus microscope.

Images from GSDMD-GFP expressing tumors that had been stained were processed with FiJi (v2.0.0-rc-69/1.52i). For every tumor 3-4 regions of interest (ROI) were selected based on GFP expression blindly to the other channels. For every ROI, DAPI channel was used for segmentation using the Trainable Weka Segmentation (v3.2.29) plugin. The generated mask was used to measure the mean intensity in each cell of every marker. Cell populations were called based on level of expression of each marker (2000 au for CD3 and CD8 and 3000 au for MHCII and CD11c). Total number of cells was normalized by ROI area in mm^2.

Please cite this article in press as: Fontana et al., Small-molecule GSDMD agonism in tumors stimulates antitumor immunity without toxicity, Cell (2024), https://doi.org/10.1016/j.cell.2024.08.007

QUANTIFICATION AND STATISTICAL ANALYSIS

A Student's t-test (two-tailed) or Mann-Whitney test was used to determine differences between two groups. One- or two-way ANOVA was used to calculate differences among multiple populations. Differences between tumor growth curves were compared by first calculating the area-under-curve values for each sample and then comparing different groups using the Student's t-test or one-way ANOVA. Type I errors were corrected by the Holm-Sidak or Dunn's multiple comparisons test. Nonparametric test was used when data did not follow a normal distribution. Significance was set at p-value $\leq$ 0.05. For all figures, *, $p \leq 0.05$, **, $p \leq 0.01$, ***, $p \leq 0.001$, ****, $p \leq 0.0001$. All statistical analyses were conducted using GraphPad Prism 8.

Supplemental figures

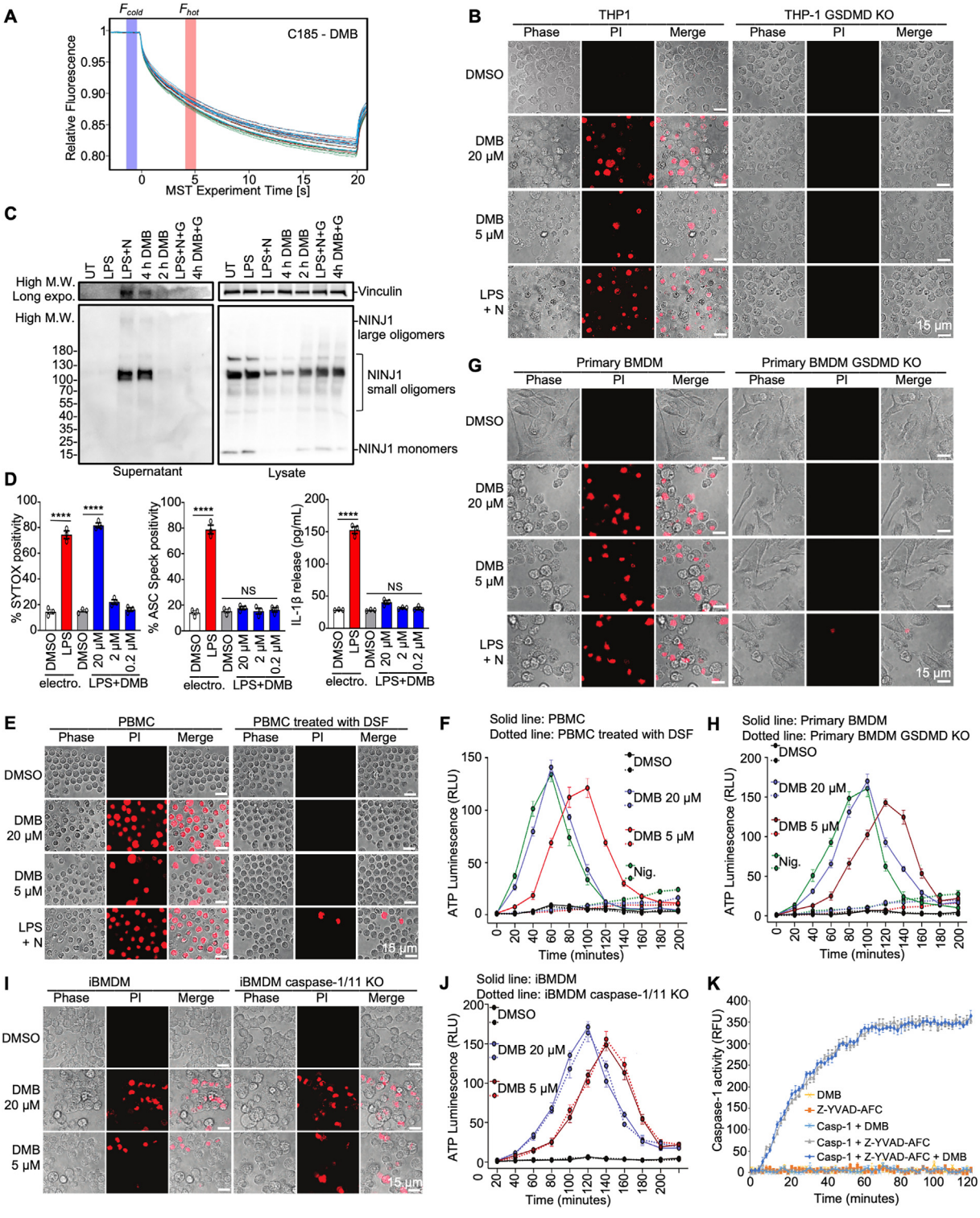

(legend on next page)

Figure S1. DMB induces pyroptosis in a GSDMD-dependent manner, related to Figures 1 and 2

(A) Microscale thermophoresis (MST) for DMB binding to GSDMD. Curves shown are fluorescence decay (F_{hot}/F_{cold}) over time for a series of DMB concentrations against a low concentration of labeled GSDMD (50 nM) when subjected to a very precise and brief laser-induced temperature change at time 0. Each curve corresponds to a ligand concentration.

(B) PI uptake (red) by WT and GSDMD KO THP-1 cells after treatment with DMSO, DMB (5 and 20 μM), or LPS + nigericin for 2 h. Scale bars, 15 μm.

(C) Anti-NINJ1 (AF5105-SP, R&D Systems) immunoblots of THP-1 supernatant and cell lysate after cells were treated with LPS + nigericin or DMB on non-reducing SDS-PAGE. N is for nigericin, and G indicates reactions performed in the presence of glycine, which inhibited NINJ1 activation.

(D) Cell death shown by SYTOX Green uptake (left), inflammasome formation is shown by ASC speck formation (middle), and effector activation is shown by IL-1β release (right). LPS electroporation (electro), but not LPS priming + DMB treatment, induced ASC speck formation and IL-1β release in THP-1 cells.

(E) PI uptake (red) by human PBMCs after treatment with DMSO, DMB (5 and 20 μM), or LPS + nigericin (Nig.) for 2 h, with or without pretreatment with the GSDMD inhibitor disulfiram (DSF). Scale bars, 15 μm.

(F) Time course of extracellular ATP measured by a luciferase-based assay in PBMCs treated with DMSO, DMB (5 and 20 μM), or LPS + nigericin, with or without pretreatment by DSF.

(G) PI uptake (red) by WT and GSDMD KO primary mouse bone-marrow-derived macrophages (BMDMs) after treatment with DMSO, DMB (5 and 20 μM), or LPS + nigericin (Nig.) for 2 h. Scale bars, 15 μm.

(H) Time course of extracellular ATP measured by a luciferase-based assay in WT and GSDMD KO primary mouse BMDMs treated with DMSO, DMB (5 and 20 μM), or LPS + nigericin.

(I) PI uptake (red) by WT and caspase-1/11 KO mouse immortalized bone-marrow-derived monocytes (iBMDMs) treated with DMSO or DMB (5 and 20 μM) for 2 h. Scale bars, 15 μm.

(J) Time course of extracellular ATP measured by luciferase-based assay in WT and caspase-1/11 KO iBMDMs treated with DMSO or DMB (5 and 20 μM) for 2 h.

(K) DMB (10 μM) does not inhibit caspase-1 (0.5 μM) activity against its fluorogenic substrate Z-YVAD-AFC (10 μM), shown by time-resolved fluorescence intensity (delay 50 μs, interval 950 μs) of each well measured at 550 nm with an excitation of 400 nm. Reaction buffer contained 40 mM HEPES, pH 7.4, 150 mM NaCl. RFU, relative fluorescence unit.

Error bars represent SEM of 3 independent experiments. NS, not significant; $^{****}p < 0.0001$.

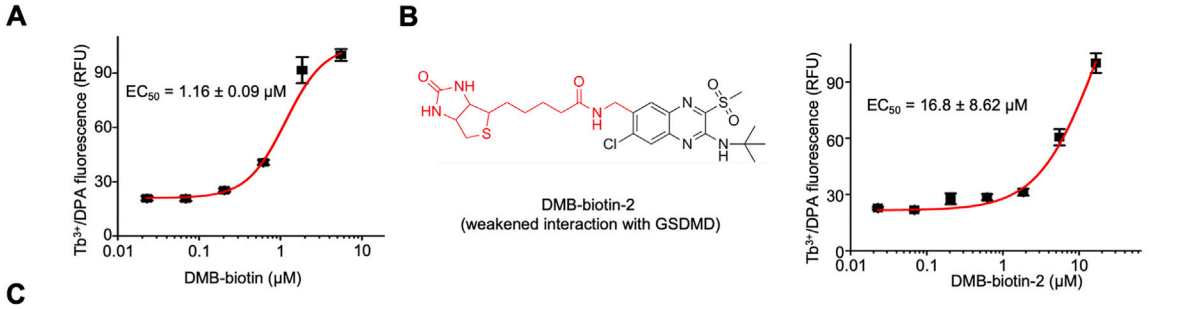

C

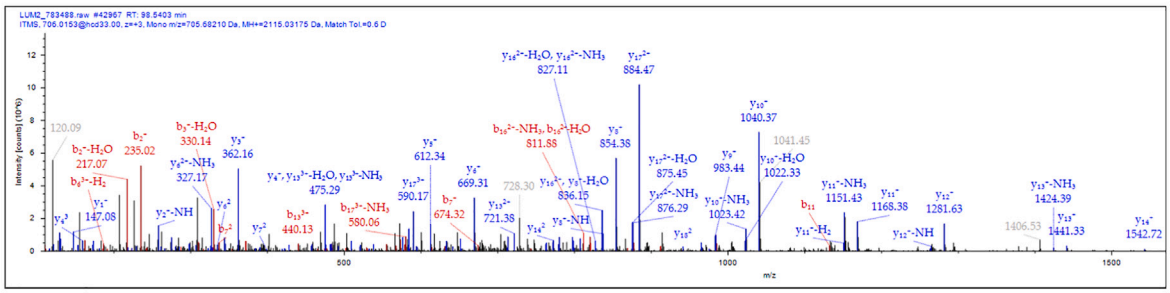

D

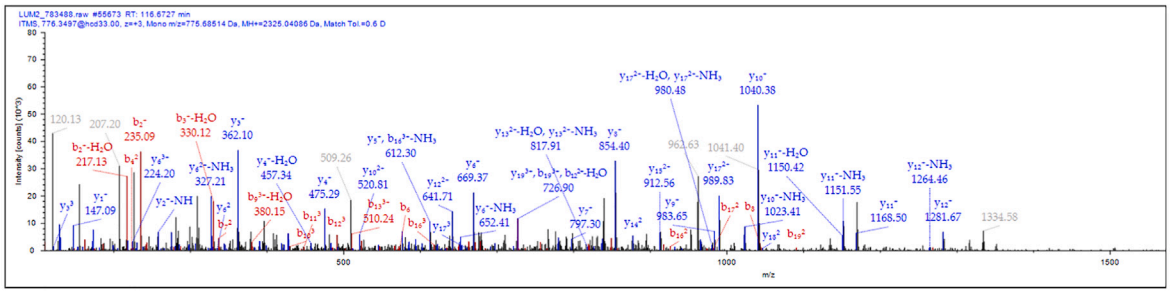

E

```
hGSDMD MGSAFERVVRRVVQELD-HGGEFIPVTSLQSSTGFQPYCLVVRKPSSSWFWKPRYKCVNL  59
mGSDMD MPSAFEKVVKNVIKEVSGSRGDLIPVDSLRNSTSFRPYCLLNRKFSSSRFWKPRYSCVNL  60
                                                 Cys38
hGSDMD SIKDILEPDAAEPDVQRGRSFHFYDAMDGQIQGSVELAAPGQAKIAGGAAVSDSSSTSMN  119
mGSDMD SIKDILEPSAPEPEPECFGSFKVSDVVDGNIQGRVMLSGMGEGKISGGAAVSDSSSASMN  120

hGSDMD VYSLSVDPNTWQTLLHERHLRQPEHKVLQQLRSRGDNVYVVTEVLQTQKEVEVTRTHKRE  179
mGSDMD VCILRVTQKTWETMQHERHLQQPENKILQQLRSRGDDLFVVTEVLQTKEEVQITEVHSQE  180

hGSDMD GSGRFSLPGATCLQGEGQGHLSQKKTVTIPSGSTLAFRVAQLVIDSDLDVLLFPDKKQRT  239
mGSDMD GSGQFTLPGALCLKGEGKGHQSRKKMVTIPAGSILAFRVAQLLIGSKWDILLVSDEKQRT  240
                                  Cys191
```

F

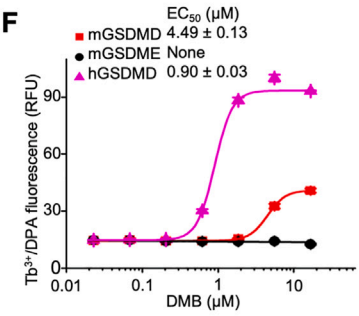

G

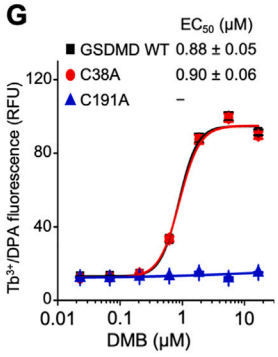

H

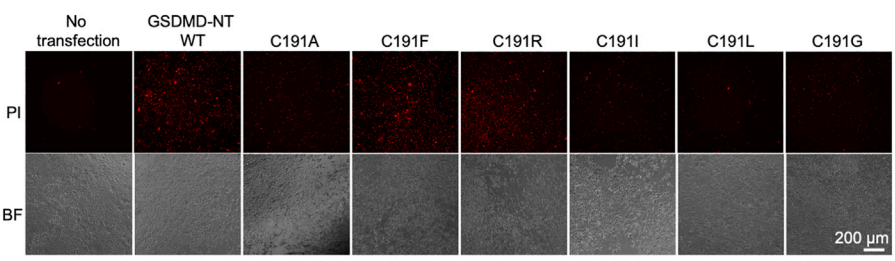

(legend on next page)

Figure S2. DMB-biotin and modification Cys191 (Cys192) of human (mouse) GSDMD by DMB, related to Figure 3

(A) GSDMD-mediated liposome leakage assay induced DMB-biotin, showing an EC_{50} similar to that of DMB.

(B) Molecular structure of another DMB-biotin conjugate (left) and its reduced induction of GSDMD-mediated liposome leakage (right).

(C and D) Nano-LC-MS/MS spectrum for the peptide containing Cys191 in human GSDMD after DMB treatment, FSLPGATCLQGEGQGHLSQK modified on cysteine by carbamidomethyl (control) (C), and FSLPGATCLQGEGQGHLSQK modified on cysteine by DMB (D). From a calculation based on the abundance values, 64.3% of Cys191 in human GSDMD was modified by DMB, while only 0.7%, 4.0%, 2.8%, 0.2%, and 0.03% of C56, C268, C309, C445, and C467 residues, respectively, were modified. Modifications of other Cys residues were not observed.

(E) Sequence alignment of the NTs of human GSDMD (hGSDMD) and mouse GSDMD (mGSDMD), highlighting the Cys residues (red).

(F) Liposome leakage assay measuring activity of DMB-treated mouse GSDMD and GSDME (mGSDMD and mGSDME) in comparison to human GSDMD (hGSDMD). The hGSDMD data are the same as in Figure 3G.

(G) Liposome leakage assay of WT C38A and C191A GSDMD activated by DMB.

(H) PI uptake (red) of HEK293T cells expressing WT and mutant GSDMD-NT. BF, brightfield image. Scale bars, 200 μm.

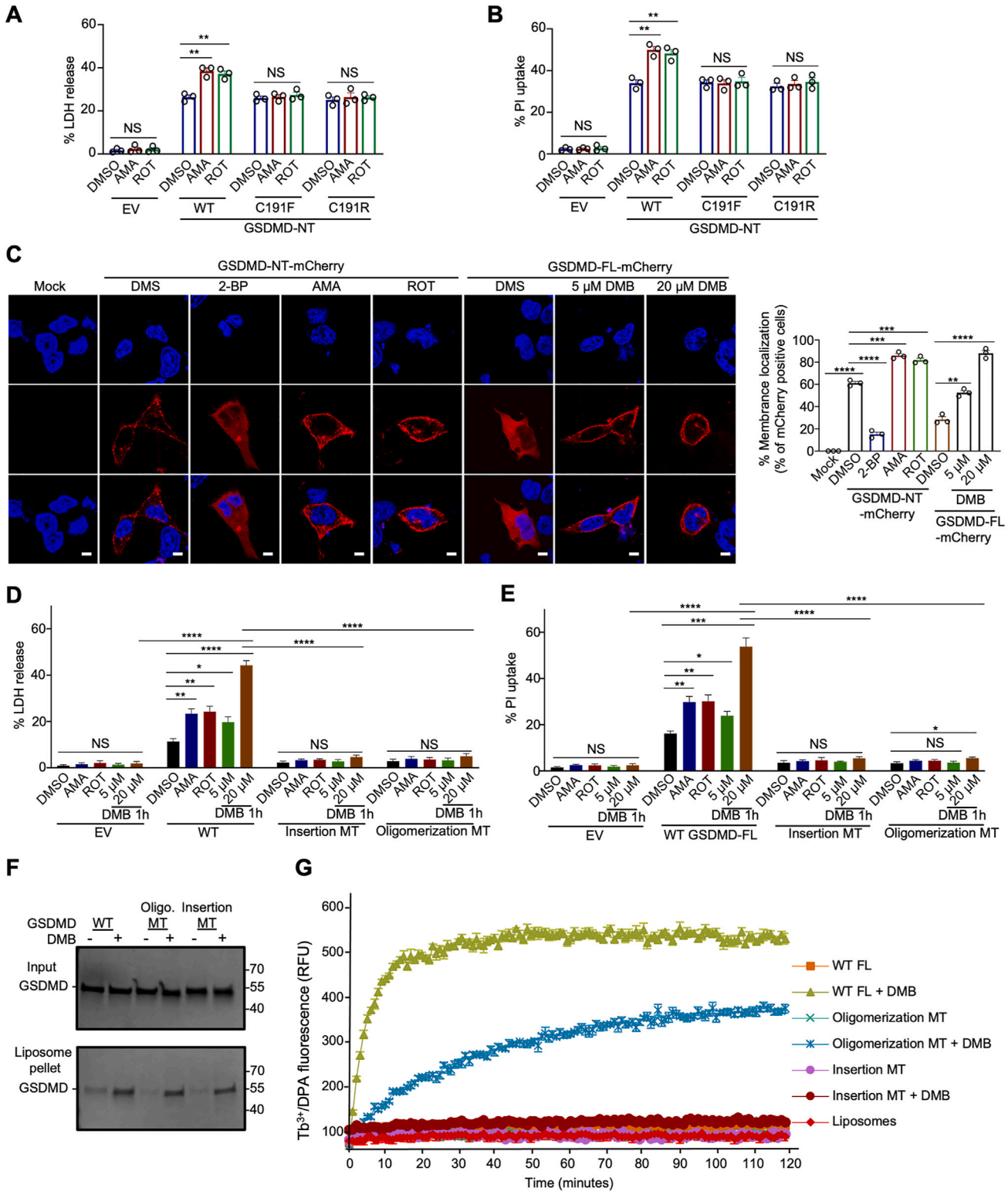

Figure S3. DMB partly mimics palmitoylation, related to Figure 3

(A and B) Quantification of LDH release (A) and PI uptake (B) of GSDMD-NT WT or C191F and C191R mutants transfected in HEK293T and treated for 2 h with DMSO, antimycin A (AMA), or rotenone (ROT). AMA and ROT enhanced cell death by WT GSDMD-NT, but not C191F and C191R mutants.

(legend continued on next page)

(C) Representative images for membrane localization (left) and quantification (right) of HEK293T cells expressing GSDMD-NT-mCherry WT treated for 4 h with DMSO, 2-BP, AMA or ROT, or GSDMD-FL-mCherry WT treated for 1 h with DMSO or DMB (5 and 20 μM). Like GSDMD-NT, GSDMD-FL showed substantial membrane localization upon DMB treatment. Scale bars represent 5 μm.
(D and E) Quantification of LDH release (D) and PI uptake (E) of GSDMD-FL WT, oligomerization mutant (K145D, R153D), insertion mutant (F184D, L186D), and control empty vector (EV) transfected in HEK293T cells and treated for 2 h with DMSO, AMA, ROT, or DMB (5 and 20 μM).
(F) Coomassie blue stained gel of liposome pull-down of recombinant GSDMD WT, oligomerization mutant (K145D, R153D), and insertion mutant (F184D, L186D), with or without DMB.
(G) Liposome leakage assay showing that DMB activates recombinant GSDMD WT, and partially activates the oligomerization mutant (K145D, R153D).

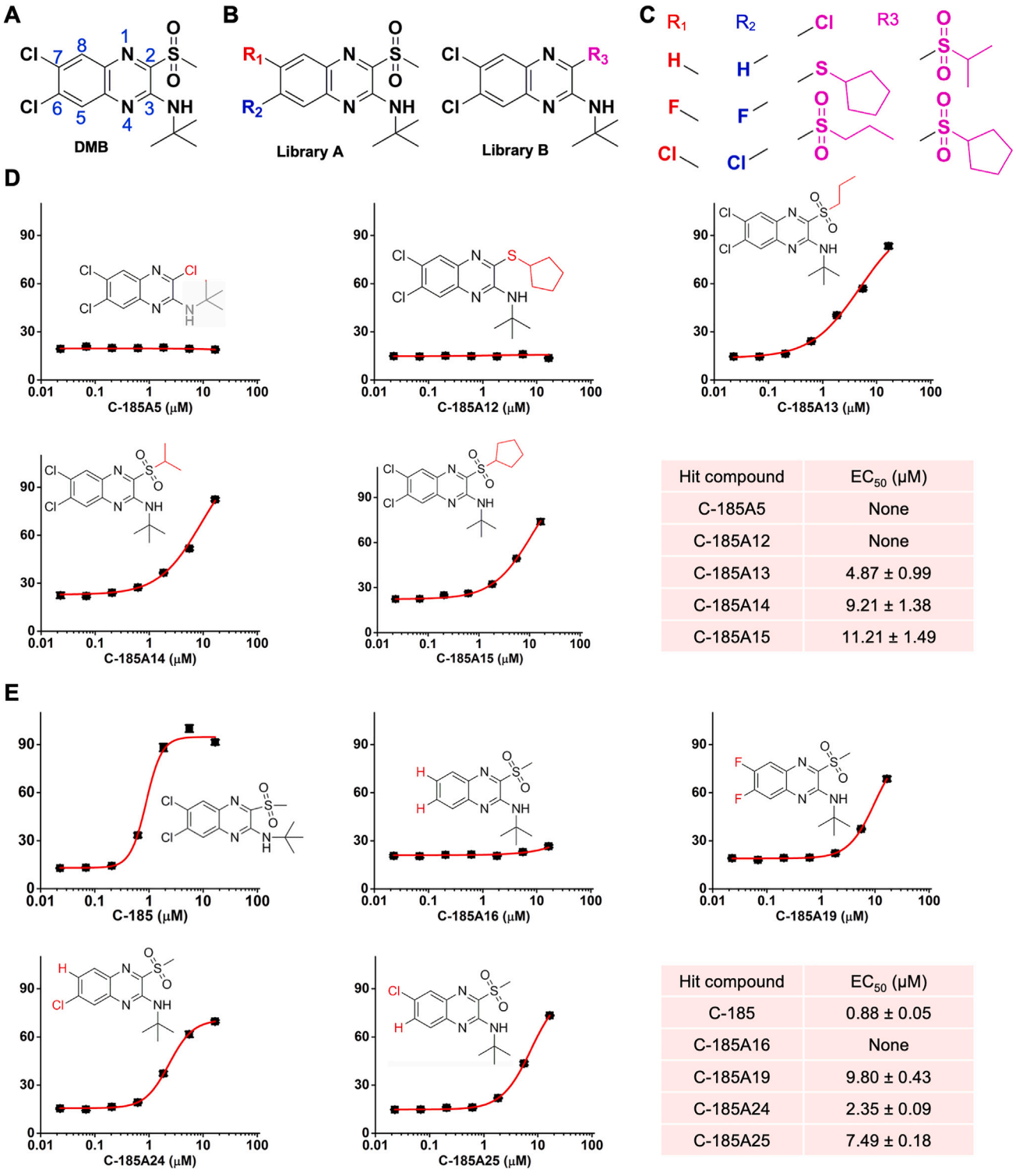

Hit compound	EC_{50} (μM)
C-185A5	None
C-185A12	None
C-185A13	4.87 ± 0.99
C-185A14	9.21 ± 1.38
C-185A15	11.21 ± 1.49

Hit compound	EC_{50} (μM)
C-185	0.88 ± 0.05
C-185A16	None
C-185A19	9.80 ± 0.43
C-185A24	2.35 ± 0.09
C-185A25	7.49 ± 0.18

Figure S4. Structure-activity relationship analysis of DMB, related to Figure 3

(A) Structure of DMB with core positions numbered.

(B) Schematic of library design with the three varied positions labeled as R1, R2, and R3.

(C) Chemical groups substituted for each library.

(D and E) GSDMD-induced liposome leakage by DMB derivatives, which were generated by changing the methylsulfonyl moiety (D) or the substitution at carbon positions 6 and 7 (E), along with molecular structure and EC_{50} (bottom right panels for both D and E).

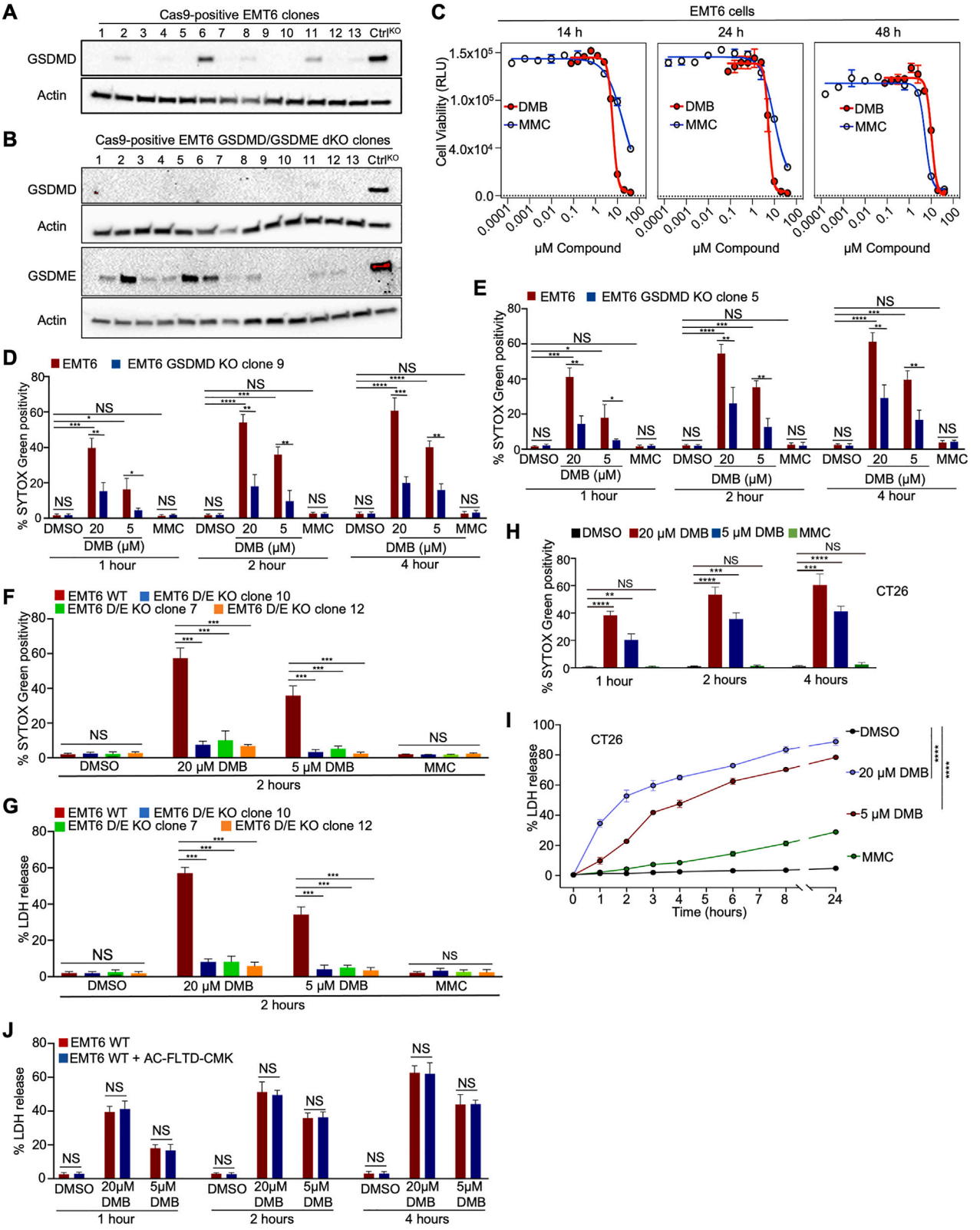

(legend on next page)

Figure S5. WT, GSDMD KO, and GSDMD/GSDME dKO EMT6 lines and the CT26 line, related to Figure 4

(A and B) Western blots of GSDMD (ab209845, abcam) and/or GSDME (ab215191, abcam) expression in Cas9-positive GSDMD KO, and GSDMD and GSDME double KO (dKO) clones, and $Ctrl^{KO}$ cells transfected with no guide. Actin (sc-47778, Santa Cruz Biotechnology) served as the loading control.

(C) Luciferase-based cell viability assay in WT EMT6 cells after incubation with indicated concentrations of DMB (red) or MMC (blue) for 14 (left), 24 (middle), or 48 (right) h. RLU, relative luminescence unit.

(D and E) Quantification of % of cells that took up SYTOX Green 1, 2, and 4 h after DMB (5 and 20 μM) or MMC (30 μM) treatment of WT and GSDMD KO clone 9 (D) and clone 5 (E), MMC-treated cells did not take up SYTOX Green.

(F) Quantification of % of cells that took up SYTOX Green 2 h after DMB (5 and 20 μM) or MMC (30 μM) treatment of WT and GSDMD/GSDME dKO (clones 7, 10, and 12) EMT6 cells. MMC-treated cells did not take up SYTOX Green.

(G) LDH release 2 h after treatment of WT and GSDMD/GSDME dKO (clones 7, 10, and 12) EMT6 cells with DMSO, DMB (5 and 20 μM), or MMC (30 μM).

(H) Quantification of % of CT26 cells that took up SYTOX Green uptake 1, 2, and 4 h after treatment with DMSO, DMB (5 and 20 μM), or MMC (30 μM).

(I) LDH release over time from CT26 cells after treatment with DMSO, MMC (30 μM), or DMB (5 and 20 μM). Note discontinuous x axis.

(J) LDH release in DMB-treated WT EMT6 cells that were pretreated or not with the inflammatory caspase inhibitor AC-FLTD-CMK. LDH release was measured 1, 2, and 4 h after adding DMB.

Error bars represent SEM of 3 independent experiments. Statistics were measured by Student's t tests. NS, not significant; $^{*}p < 0.05$, $^{**}p < 0.01$, $^{***}p < 0.001$, $^{****}p < 0.0001$.

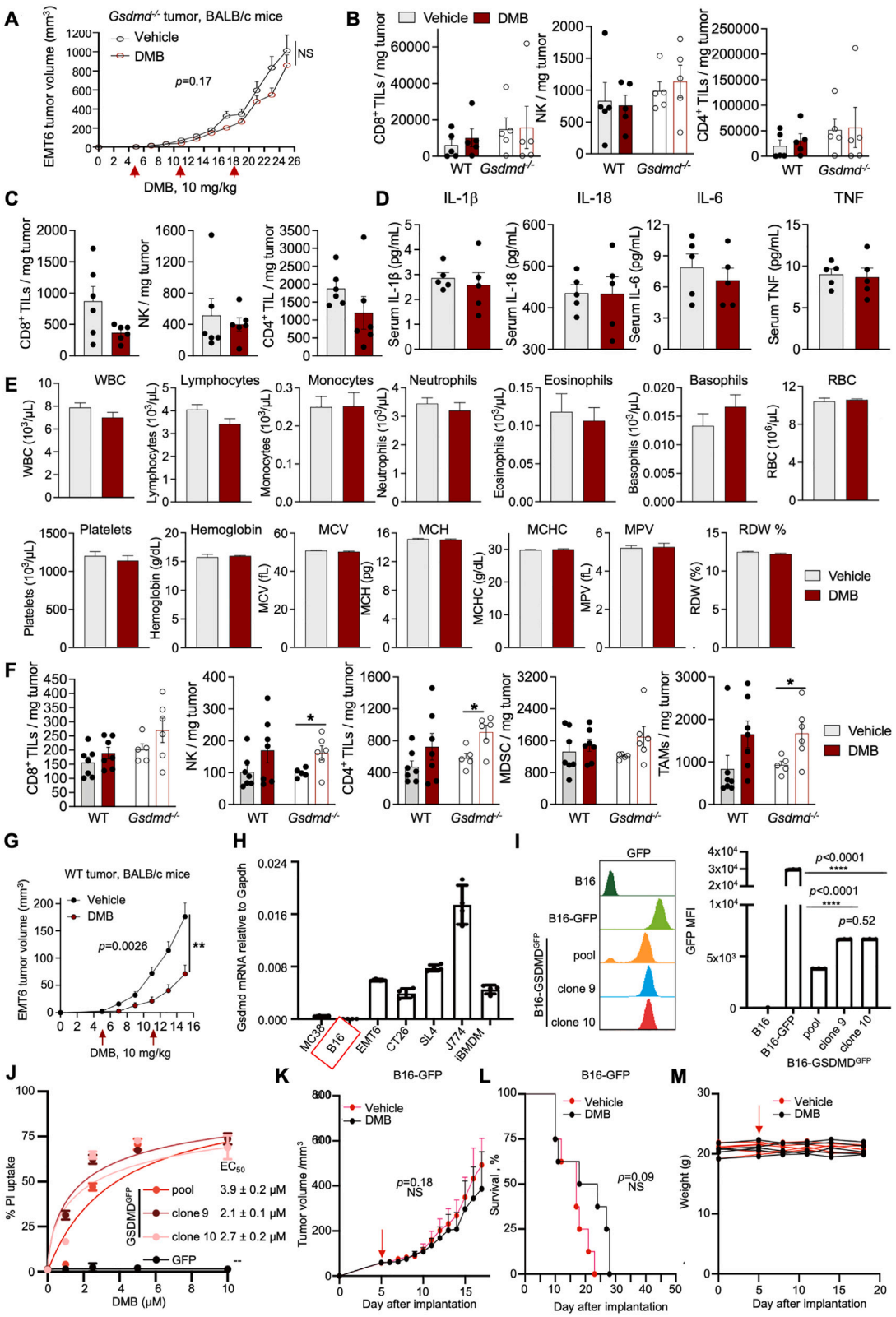

(legend on next page)

Figure S6. *In vivo* treatment of various tumors by DMB and lack of toxicity shown by blood counts or serum cytokine levels, related to Figures 5, 6, and 7

(A) Mice bearing orthotopic *Gsdmd*$^{-/-}$ EMT6 tumors were treated with vehicle or DMB (10 mg/kg) every week starting when tumors became palpable and analyzed for tumor volume.

(B) BALB/c mice orthotopically implanted with WT or *Gsdmd*$^{-/-}$ EMT6 tumors were treated with vehicle or DMB. Shown are numbers of CD8^{+} (left), NK (middle), or CD4^{+} (right) TILs. n = 5 mice/group.

(C) BALB/c mice implanted subcutaneously with CT26 were treated with vehicle or DMB. Numbers of CD8^{+} (left), NK (middle), or CD4^{+} (right) TILs were compared. n = 6 mice/group.

(D) Levels of IL-1β, IL-18, IL-6, or TNF-α in serum were compared in BALB/c mice orthotopically implanted with EMT6 tumors that were treated with vehicle or DMB. n = 5/group.

(E) Complete blood counts were compared in BALB/c mice orthotopically implanted with EMT6 tumors that were treated with vehicle or DMB. n = 5/group. WBC, white blood cells.

(F) WT or *Gsdmd*$^{-/-}$ mice implanted subcutaneously with KP tumors were treated with vehicle or DMB. Numbers of CD8^{+}, NK, or CD4^{+} TILs, myeloid-derived suppressor cells (MDSCs), and TAMs in tumors were compared. WT mice, vehicle or DMB treatment, n = 7 mice/group; *Gsdmd*$^{-/-}$ mice, vehicle treatment, n = 5 mice/group; DMB treatment, n = 6 mice/group.

Error bars represent SEM of 3 independent experiments. Statistics were measured by Student's t tests. NS, not significant; *$p < 0.05$, **$p < 0.01$, ***$p < 0.001$, ****$p < 0.0001$.

(G) DMB effect on tumor volumes in WT mice implanted with EMT6 WT tumors.

(H) *Gsdmd* mRNA in mouse cancer cell lines, assessed by RT-qPCR, relative to *Gapdh*.

(I) GFP expression of untransfected B16 and B16 transfected to ectopically express GFP or human GSDMD-GFP, analyzed by flow cytometry for GFP mean fluorescence intensity (MFI).

(J) *In vitro* PI uptake measured 2 h after adding indicated concentrations of DMB to B16-GFP or B16-GSDMD-GFP cells (pools or indicated clones). DMB EC_{50} curves were fit based on the percentage of cells that took up PI.

(K and L) Tumor growth (E) and survival (F) curves of B16-GFP tumors treated with DMB (10 mg/kg, n = 4) or vehicle (n = 4). B16-GFP cells were implanted sc on day 0, and mice were treated i.p. every 3 days for 6 injections with 10 mg/kg DMB or vehicle, starting 5 days post-implantation (red arrow) when all mice had palpable tumors. Growth curves show mean ± SEM at each time point and are representative of two independent experiments. The area under the tumor growth curves was compared by two-tailed Student's t test. Kaplan-Meier survival curve was analyzed by log-rank test (n = 8/group).

(M) Mouse weight before and after DMB (black) or vehicle (red) treatment begun on day 5 (arrow). There was no significant difference in weight between mice treated with DMB or vehicle.

NS, not significant; *$p < 0.05$, **$p < 0.01$, ***$p < 0.001$, ****$p < 0.0001$.

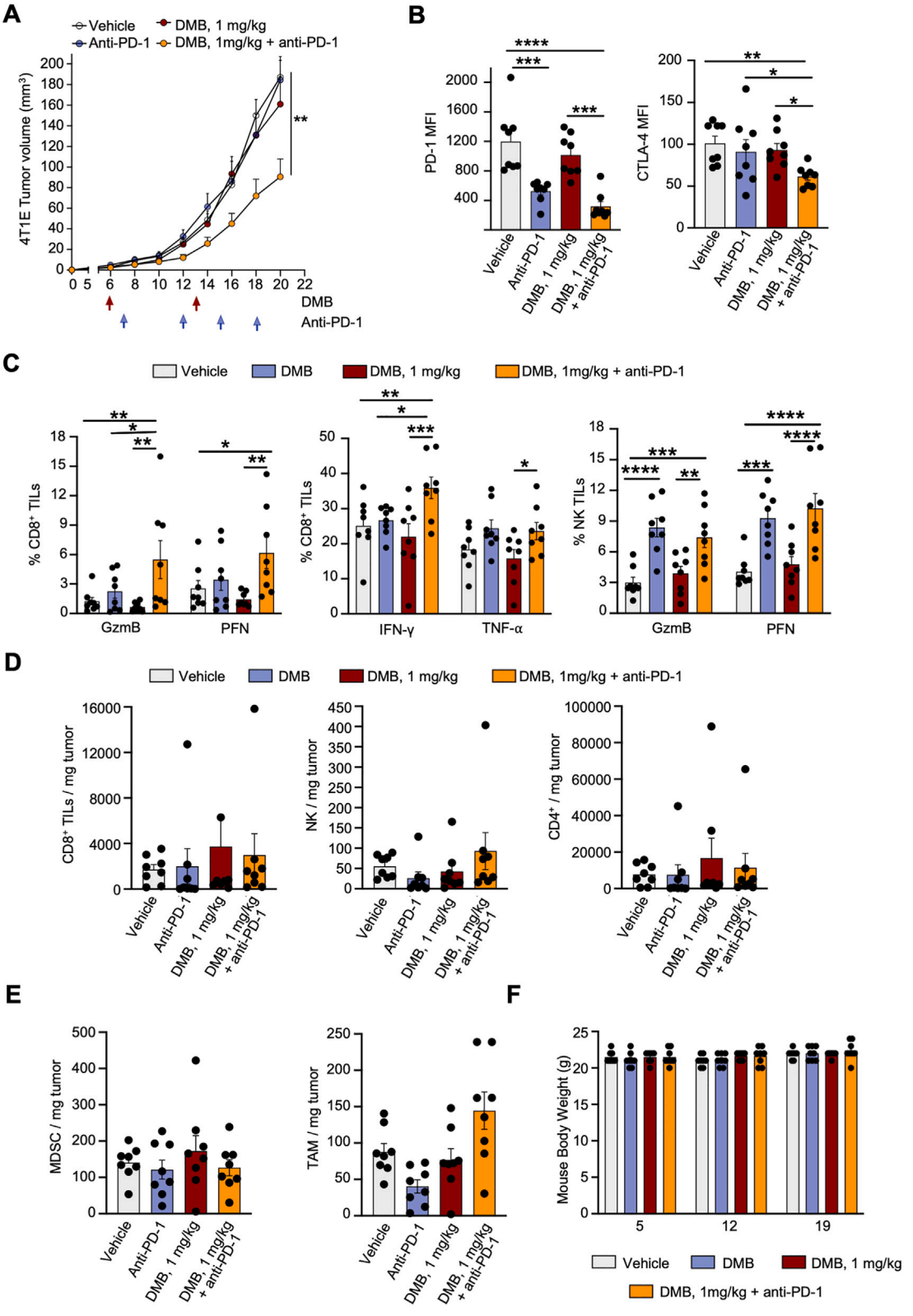

(legend on next page)

Figure S7. DMB used at low dose synergizes with anti-PD-1 to exert potent antitumor activity in 4T1E tumor model, related to Figure 7

(A) Orthotopically implanted 4T1E tumors in BALB/c mice treated with vehicle, anti-PD-1 every 2 days, DMB (1 mg/kg) every week, or anti-PD-1 combined with DMB (1 mg/kg) starting when tumors became palpable and analyzed for tumor volume. $n = 8$ mice/group.

(B) Expression of co-inhibitory molecules PD-1 and CTLA-4 on antigen-experienced $CD44^+$-$CD8^+$ TILs in each group of tumors on day 21 (end of the study). MFI, mean fluorescence intensity.

(C) Percentages of $CD8^+$ TILs expressing GzmB or PFN (left), or IFN-γ or TNF-α after PMA and ionomycin stimulation *ex vivo* (middle), and percentages of NK^+ TILs expressing GzmB or PFN (right).

(D) Numbers of $CD8^+$, NK, or $CD4^+$ TILs in tumors compared between vehicle, anti-PD-1, DMB, or DMB + anti-PD-1 treatments.

(E) Numbers of myeloid-derived suppressor cells (MDSC), and tumor-associated macrophages (TAMs) in tumors compared between vehicle, anti-PD-1, DMB, or DMB + anti-PD-1 treatments.

(F) Animal body weight at different time points before and after vehicle, anti-PD-1, DMB, and anti-PD-1 + DMB treatments.

All data are represented as mean ± SEM. For tumor volume analysis, the area under the tumor growth curves was compared by a two-tailed Student's t test. For expression analyses, one- or two-way ANOVA was used to calculate differences among the different groups. $^*p < 0.05$, $^{**}p < 0.01$, $^{***}p < 0.001$, $^{****}p < 0.0001$.